

## ARTICLE

# PQLC2 recruits the C9orf72 complex to lysosomes in response to cationic amino acid starvation

Joseph Amick<sup>1,2,3</sup>, Arun Kumar Tharkeshwar<sup>1,2,3</sup>, Gabriel Talaia<sup>1,2,3</sup>, and Shawn M. Ferguson<sup>1,2,3</sup>

**The C9orf72 protein is required for normal lysosome function. In support of such functions, C9orf72 forms a heterotrimeric complex with SMCR8 and WDR41 that is recruited to lysosomes when amino acids are scarce. These properties raise questions about the identity of the lysosomal binding partner of the C9orf72 complex and the amino acid-sensing mechanism that regulates C9orf72 complex abundance on lysosomes. We now demonstrate that an interaction with the lysosomal cationic amino acid transporter PQLC2 mediates C9orf72 complex recruitment to lysosomes. This is achieved through an interaction between PQLC2 and WDR41. The interaction between PQLC2 and the C9orf72 complex is negatively regulated by arginine, lysine, and histidine, the amino acids that PQLC2 transports across the membrane of lysosomes. These results define a new role for PQLC2 in the regulated recruitment of the C9orf72 complex to lysosomes and reveal a novel mechanism that allows cells to sense and respond to changes in the availability of cationic amino acids within lysosomes.**

## Introduction

A hexanucleotide repeat expansion in a noncoding region of the C9orf72 gene causes familial forms of amyotrophic lateral sclerosis and frontotemporal dementia (DeJesus-Hernandez et al., 2011; Gijssels et al., 2012; Renton et al., 2011). Although the repeat expansion results in a reduction in C9orf72 mRNA and protein levels, the extent to which this is relevant for disease pathogenesis remains unclear (Belzil et al., 2013; DeJesus-Hernandez et al., 2011; Gijssels et al., 2012; Shi et al., 2018; Viodé et al., 2018; Waite et al., 2014; Xi et al., 2013). Nonetheless, investigation of this topic has established that the C9orf72 protein is required for normal lysosome homeostasis in a variety of model systems, including mice, *Caenorhabditis elegans*, and cultured human cells (Amick et al., 2016; Corriero and Horvitz, 2018; McAlpine et al., 2018; O'Rourke et al., 2016; Sullivan et al., 2016; Zhang et al., 2018). Thus, beyond potential neurodegenerative disease implications, C9orf72 has an evolutionarily conserved role in supporting lysosome function.

The C9orf72 protein is unstable on its own and functions as part of a larger protein complex that also contains SMCR8 and WDR41 (Amick et al., 2016; Sellier et al., 2016; Sullivan et al., 2016; Ugolino et al., 2016; Xiao et al., 2016). Consistent with a direct function at lysosomes, this C9orf72 protein complex localizes to the cytoplasmic surface of lysosomes (Amick et al., 2016, 2018). Interestingly, interactions between the C9orf72 complex and lysosomes are acutely regulated by changes in

amino acid availability and are most prominent when cells are deprived of amino acids (Amick et al., 2016, 2018). Although there is now considerable evidence for a lysosomal site of action, the mechanisms that support the regulated recruitment of the C9orf72 complex to lysosomes in response to amino acid scarcity have remained unsolved.

In addition to their classically defined role in the breakdown of cellular macromolecules, lysosomes also possess signaling functions. This is best appreciated in the context of the mTORC1 signaling pathway, a central pathway for the regulation of cell growth and metabolism (Shimobayashi and Hall, 2014). Amino acid availability is a key factor regulating mTORC1 activation. mTORC1 is recruited to lysosomes via binding to the Rag GTPases, whose nucleotide loading status is regulated by amino acid availability (Bar-Peled and Sabatini, 2014). Multiple lysosomal proteins have been identified that function as sensors for specific amino acids and are integrated into signaling pathways that converge on the Rags (Wolfson and Sabatini, 2017). Although investigation of mTORC1 regulation has contributed significantly to our understanding of how amino acid availability is sensed at lysosomes and communicated to mTORC1 via the Rag GTPases, C9orf72 has not been implicated in regulation of the Rag GTPase pathway. This suggests the existence of an undefined amino acid-sensing mechanism that operates upstream of the C9orf72 complex at lysosomes.

<sup>1</sup>Department of Cell Biology, Yale University School of Medicine, New Haven, CT; <sup>2</sup>Department of Neuroscience, Yale University School of Medicine, New Haven, CT; <sup>3</sup>Program in Cellular Neuroscience, Neurodegeneration and Repair, Yale University School of Medicine, New Haven, CT.

Correspondence to Shawn M. Ferguson: [shawn.ferguson@yale.edu](mailto:shawn.ferguson@yale.edu).

© 2019 Amick et al. This article is distributed under the terms of an Attribution-Noncommercial-Share Alike-No Mirror Sites license for the first six months after the publication date (see <http://www.rupress.org/terms/>). After six months it is available under a Creative Commons License (Attribution-Noncommercial-Share Alike 4.0 International license, as described at <https://creativecommons.org/licenses/by-nc-sa/4.0/>).

In this study, we identify proline-glutamine loop containing 2 (PQLC2), a lysosomal transporter of cationic amino acids (Jézégou et al., 2012; Liu et al., 2012), as an interactor of the C9orf72 complex and find that PQLC2 mediates the recruitment of the C9orf72 complex to lysosomes. The interaction between PQLC2 and the C9orf72 complex is specifically regulated by the availability of arginine, lysine, and histidine, the amino acids transported by PQLC2. Collectively, these results define a mechanism for amino acid-regulated recruitment of the C9orf72 complex to lysosomes and reveal a new pathway whereby the status of the lysosomal lumen is communicated to the rest of the cell.

## Results

### Identification of PQLC2 as a lysosomal binding partner for the C9orf72 complex

To understand how the C9orf72 complex is recruited to lysosomes in response to amino acid starvation, we sought to identify lysosomal binding partners of the C9orf72 complex. Although the endogenous C9orf72 protein is found on lysosomes in starved cells (Amick et al., 2016, 2018), its low expression levels raised challenges for the detection of lysosomal interacting partners of C9orf72. We therefore took advantage of a lysosome-targeted C9orf72 chimera, which was made by fusing the first 39 amino acids of p18/LAMTOR1 to C9orf72-GFP (Fig. 1 A). This region of LAMTOR1 contains an acidic dileucine motif, palmitoylation and myristoylation sites, and can be used to target proteins fused to it to the cytoplasmic surface of lysosomes (Amick et al., 2018; Menon et al., 2014; Nada et al., 2009). Fusion of this region of LAMTOR1 to C9orf72-GFP was previously demonstrated to support the efficient targeting of a functional C9orf72 protein to the cytoplasmic surface of lysosomes (Amick et al., 2018). We therefore used lysosome-targeted C9orf72 (Lyso-C9orf72-GFP) as bait in immunoprecipitation experiments to identify lysosome-localized binding partners of the C9orf72 complex (Fig. 1 B). Parallel anti-GFP immunoprecipitations from cells coexpressing Lyso-C9orf72-GFP and SMCR8-tdTomato or control cells expressing lysosome-targeted GFP (Lyso-GFP; Fig. 1 A) and SMCR8-tdTomato were analyzed by mass spectrometry (MS). This approach identified multiple proteins that were selectively enriched in the Lyso-C9orf72-GFP sample (Fig. 1 C), including known C9orf72 interactors such as SMCR8, WDR41, and the ULK1 complex (ULK1, RBICC1, ATG13, and ATG101; Amick et al., 2016; Jung et al., 2017; Sellier et al., 2016; Sullivan et al., 2016; Xiao et al., 2016; Yang et al., 2016). We also identified PQLC2, an amino acid transporter responsible for the efflux of cationic amino acids from lysosomes (Jézégou et al., 2012; Liu et al., 2012), in the Lyso-C9orf72-GFP samples (Fig. 1 C). This amino acid transporter was particularly interesting given that C9orf72 complex abundance at lysosomes is regulated by changes in amino acid availability (Amick et al., 2016, 2018).

To further evaluate the interaction between PQLC2 and the C9orf72 complex, we performed immunoprecipitations on cells transfected with FLAG-tagged PQLC2 and found that it interacts with the endogenously expressed C9orf72 and SMCR8 (Fig. 1 D). As evidence of the specificity for the binding between PQLC2

and the C9orf72 complex, no interaction (Fig. 1 D) was detected between C9orf72 or SMCR8 and FLAG-tagged PAT1 (also known as LYAAT1 and SLC36A1), a lysosomal amino acid transporter of small neutral amino acids (Sagné et al., 2001). Both the PQLC2-FLAG and FLAG-PAT1 proteins colocalize with LAMP1 on late endosomes and lysosomes (Fig. S1, A and B).

To assess colocalization between C9orf72 and PQLC2, cells that express 2xHA-tagged C9orf72 from the endogenous locus were transiently transfected to express FLAG-tagged PQLC2 under the control of the strong cytomegalovirus promoter. In starved cells, C9orf72 localized to PQLC2-positive lysosomes (Fig. 1 E). Surprisingly, the overexpression of PQLC2 drove localization of C9orf72 to lysosomes even in fed cells (Fig. 1 E). In contrast, overexpression of PAT1 did not noticeably alter C9orf72 localization (Fig. 1 F). The coimmunoprecipitation between C9orf72 and PQLC2 and the powerful effects of PQLC2 overexpression on C9orf72 localization suggested that interactions with PQLC2 mediate the recruitment of C9orf72 to lysosomes.

### PQLC2 is required for C9orf72 complex association with lysosomes

To test if PQLC2 is essential for C9orf72 recruitment to lysosomes, we used CRISPR-Cas9 to knock out PQLC2 in HEK293FT cells. After isolating clonal cell populations, we sequenced the PQLC2 locus and identified a line with frameshift deletions (7-bp and 34-bp deletions at the sgRNA target site in PQLC2 exon 2) and the absence of any remaining WT PQLC2 sequences. We then performed immunofluorescence analysis and found that C9orf72 was no longer recruited to lysosomes in response to starvation in PQLC2 knockout (KO) cells (Fig. 2, A and B).

C9orf72 and SMCR8 are predicted to be structurally similar to the folliculin (FLCN) and FLCN-interacting proteins (FNIPs), which also form a complex that is recruited to lysosomes in starved cells (Amick and Ferguson, 2017; Amick et al., 2016; Meng and Ferguson, 2018; Petit et al., 2013). To test the specificity of the requirement for PQLC2 in the lysosomal recruitment of the C9orf72 complex, we next examined FLCN localization in PQLC2 KO cells using an FLCN antibody that was previously established to yield a specific lysosomal immunofluorescence signal (Meng and Ferguson, 2018). Although C9orf72 and FLCN both exhibit a punctate distribution in starved WT cells, only FLCN still shows this punctate, LAMP1 colocalized, distribution in PQLC2 KO cells (Fig. 2, C and D). These experiments reveal specificity in the role for PQLC2 on C9orf72 regulation.

Amino acid availability is communicated to FLCN via amino acid sensors upstream of the GATOR1 complex, and cells lacking the Nprl3 subunit of GATOR1 are unable to recruit FLCN to lysosomes (Meng and Ferguson, 2018). To test the role for GATOR1 in communicating amino acid availability to C9orf72, we next knocked out Nprl3 in the background of a CRISPR knockin cell line that expresses 2xHA-C9orf72 from the endogenous locus. As expected, these cells are unable to efficiently inactivate mTORC1 during amino acid starvation (Fig. S2 A; Bar-Peled et al., 2013; Panchaud et al., 2013). Unlike FLCN, C9orf72 was still recruited to lysosomes in starved Nprl3 KO cells (Fig. S2, B and C). Thus,

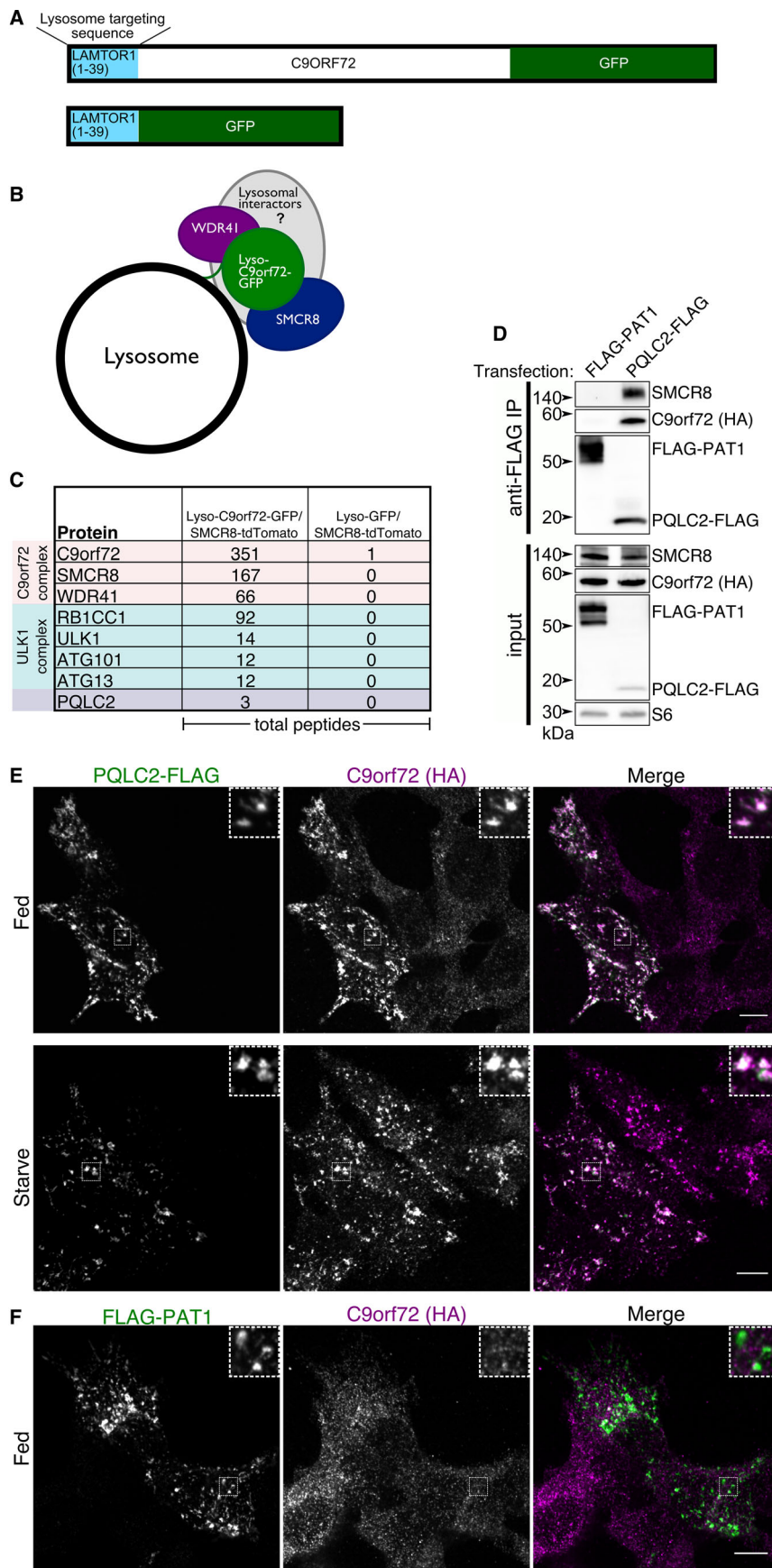


**Figure 1. Identification of the amino acid transporter PQLC2 as a C9orf72-interacting protein.** **(A)** Schematic diagram illustrating the Lyso-C9orf72-GFP and the Lyso-GFP proteins that were used for proteomics experiments. **(B)** Summary of strategy to enrich the C9orf72 complex at lysosomes to facilitate identification of lysosomal-interacting partners. **(C)** Summary of proteins identified by LC-MS/MS that interact with Lyso-C9orf72-GFP compared with a Lyso-GFP control. Total peptide numbers are shown. **(D)** HEK293FT cells that express 2xHA-tagged C9orf72 from the endogenous locus were transfected with FLAG-tagged PQLC2 or FLAG-PAT1, followed by anti-FLAG immunoprecipitation and immunoblotting for FLAG or endogenously expressed SMCR8 and C9orf72. **(E)** Effect of PQLC2 overexpression on C9orf72 localization in fed and starved cells. Scale bars: 10  $\mu$ m. Insets: 6.0  $\mu$ m wide. **(F)** PAT1 overexpression did not affect C9orf72 localization in fed cells. Scale bar: 10  $\mu$ m. Inset: 5.6  $\mu$ m wide.

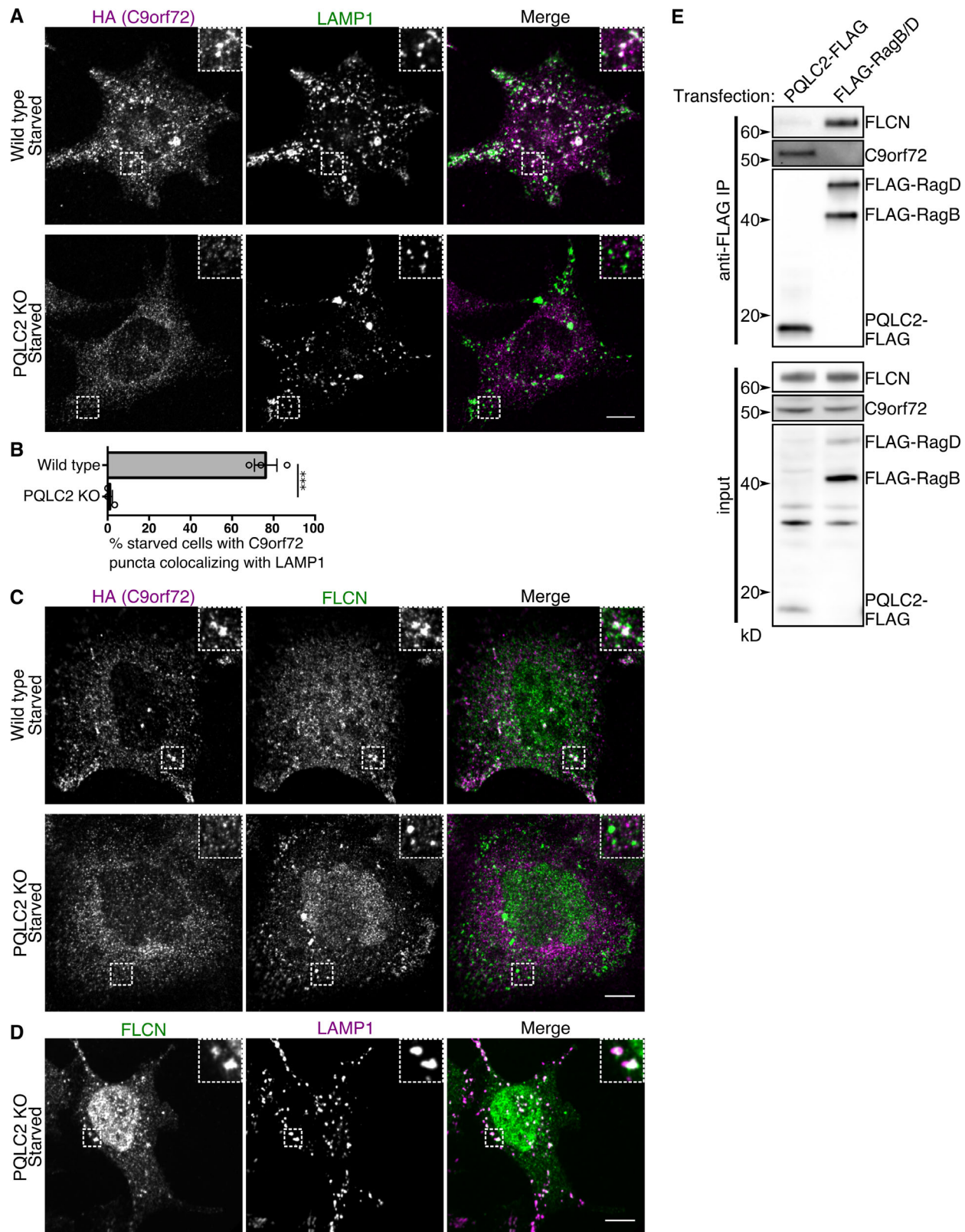


Figure 2. **PQLC2 is required for C9orf72 recruitment to lysosomes.** (A) Immunofluorescence images of C9orf72 localization (endogenously expressed 2xHA-C9orf72) in starved WT and PQLC2 KO cells. Localization of C9orf72 to lysosomes (LAMP1) is lost in PQLC2 KO cells. Scale bar: 10  $\mu$ m. Insets: 8.0  $\mu$ m wide. (B) For the indicated cell lines, a summary of the percentage of cells in starved conditions containing C9orf72 puncta that colocalize with LAMP1. Mean  $\pm$  SEM is plotted with individual experiments displayed as open dots. Unpaired two-tailed t test; \*\*\*,  $P = 0.0002$ ,  $n = 3$ , experiments with >140 cells analyzed per cell line. (C) Immunofluorescence images of C9orf72 and FLCN localization in starved WT and PQLC2 KO cells. Scale bar: 10  $\mu$ m. Insets: 7.6  $\mu$ m wide. (D) Immunofluorescence images of FLCN localization in starved PQLC2 KO cells. Recruitment of FLCN to lysosomes (LAMP1-positive puncta) is maintained in these cells. Scale bars: 10  $\mu$ m. Inset: 6.3  $\mu$ m wide. (E) Cells expressing either PQLC2-FLAG or FLAG-tagged RagB and RagD were subjected to anti-FLAG immunoprecipitations and immunoblotting for FLAG and endogenous C9orf72 and FLCN.

although both FLCN and C9orf72 are recruited to lysosomes in response to amino acid starvation, they are recruited via different mechanisms. In addition, C9orf72 coimmunoprecipitates with PQLC2, while FLCN does not, and FLCN coimmunoprecipitates with RagB and RagD, while C9orf72 does not (Fig. 2 E). These results are consistent with a PQLC2-dependent lysosome-recruitment mechanism for C9orf72 that is distinct from the Rag-dependent recruitment mechanism for FLCN.

### **Conserved prolines in PQLC2 are required for its interaction with the C9orf72 complex**

PQLC2 contains two conserved PQ motifs (Fig. S3 A). In related transporters, the proline residues within this motif act as hinges within transmembrane helices that support conformational changes that are critical for the transport cycle (Lee et al., 2015). Replacement of these prolines with leucines was previously shown to nearly abolish PQLC2 transport of amino acids (Liu et al., 2012). We therefore tested if these residues are required for the interaction between PQLC2 and the C9orf72 complex by performing coimmunoprecipitation experiments. C9orf72, SMCR8, and WDR41 copurified with WT PQLC2 to a similar degree in fed and starved conditions, while the interactions between the C9orf72 complex and the PQLC2 P55L, P201L, and P55L/P201L double mutants were greatly reduced (Fig. 3 A).

As a complementary approach to test the role of PQLC2 and PQ loop mutants in the recruitment of C9orf72 to lysosomes, we analyzed lysosomes purified from WT, PQLC2 KO, and KO cells reconstituted with WT PQLC2-FLAG or the P55L/P201L double mutant. Lysosomes were endocytically loaded with iron dextran nanoparticles and then subjected to a magnetic purification protocol (Amick et al., 2018; Tharkeshwar et al., 2017). Following lysosome isolation, C9orf72 and SMCR8 were detected on lysosomes in WT, but not PQLC2 KO, cells (Fig. 3, B and C). The presence of C9orf72 and SMCR8 on lysosomes was restored when WT PQLC2-FLAG was added back to KO cells. However, the P55L/P201L mutant failed to rescue recruitment of the C9orf72 complex to lysosomes (Fig. 3, B–D). The impact of PQLC2 PQ-motif mutations on lysosome recruitment of C9orf72 was further corroborated by immunofluorescence experiments. Although WT PQLC2 conferred constitutive lysosome localization to C9orf72 in the PQLC2 KO cells (Fig. 3 E), expression of P55L or P201L single mutants in PQLC2 KO cells showed a much-reduced ability to support C9orf72 recruitment to lysosomes in either the fed or starved states (Fig. 3, F and G), while the P55L/P201L double mutant failed to recruit C9orf72 (Fig. 3 H).

Based on previous structural and functional studies (Lee et al., 2015; Liu et al., 2012), the failure of the PQLC2 P55L/P201L double mutant to interact with C9orf72 and rescue its recruitment to lysosomes could result from the mutant being locked in a conformation that is not favorable for interacting with the C9orf72 complex. An alternative possibility is that the P55L/P201L mutant may not traffic properly to lysosomes. However, defects in P55L/P201L trafficking were not supported by the results of our immunoblot analysis of purified lysosomes as the C9orf72 and SMCR8 lysosome recruitment defect remained apparent, even after normalizing C9orf72 and SMCR8 levels on purified lysosomes to the abundance of PQLC2 in these

samples (Fig. 3 D). Furthermore, immunofluorescence assays revealed similar levels of lysosome localization for WT PQLC2 and the proline to leucine mutants (Figs. S1 A and S3, B–D). This conclusion was further supported by quantitative analysis, which detected similar robust colocalization between WT PQLC2 and the P55L/P201L mutant with LAMP1 (Fig. S3 G). Meanwhile, both the WT and mutant PQLC2 colocalized equally poorly with calnexin, a marker of the endoplasmic reticulum (Fig. S3, E–G). Collectively, the results of immunofluorescence, lysosome purification, and coimmunoprecipitation experiments establish that (1) the interaction between PQLC2 and the C9orf72 complex is essential for its recruitment to lysosomes, and (2) the PQ motifs that are predicted to support PQLC2 conformational changes that accompany substrate transport are also critical for supporting the C9orf72 complex binding to PQLC2.

### **Cationic amino acids regulate the interaction between PQLC2 and the C9orf72 complex**

Localization of the C9orf72 complex to lysosomes is regulated by amino acid availability; this implies that the interaction with PQLC2 should also be regulated by amino acid availability. However, overexpressed PQLC2 interacted with the C9orf72 complex constitutively, with only a modest difference between fed and starved conditions (Figs. 1 E and 3 A). To overcome issues related to overexpression, we used genome editing to insert a 2xHA epitope tag into the endogenous PQLC2 gene in HEK293FT cells to yield cells that express PQLC2 with a C-terminal 2xHA epitope tag from the endogenous locus. The successful insertion of the tag was confirmed by sequencing of genomic DNA (Fig. S4, A and B). The PQLC2-2xHA cell line yielded a specific HA immunofluorescence signal that localized to lysosomes (Fig. S4, C and D). We then immunoprecipitated PQLC2 from these cells under different nutrient conditions. Cells were cultured in media with or without dialyzed serum and/or the MEM amino acids mix. The withdrawal of amino acids, but not serum, stimulated the interaction between PQLC2 and all three components of the C9orf72 complex (Fig. 4, A and B). We next asked which amino acids regulate the interaction. The MEM-amino acids solution contains 12 amino acids, including the substrates for PQLC2 (arginine, lysine, and histidine; Fig. 4 C). Cells were cultured in media containing the MEM amino acids, media lacking all amino acids, media containing just arginine, lysine, and histidine, or media lacking just arginine, lysine, and histidine. Relative to cells cultured in the presence of the complete MEM-amino acids solution, the interaction with PQLC2 was similarly increased in cells starved of all amino acids or cells that were only starved of just arginine, lysine, and histidine. However, the interaction was not stimulated when cells were starved of the other nine MEM amino acids (Fig. 4, D and E).

We next performed the reciprocal experiment, wherein cells were first starved of all amino acids to promote interactions of the C9orf72 complex with PQLC2 and were then measured for their response to the refeeding with specific amino acids. The complete MEM mixture reduced the interaction with PQLC2, as did the mix of arginine, lysine, and histidine (Fig. 4, F and G). In contrast, addition of the nine remaining amino acids did not

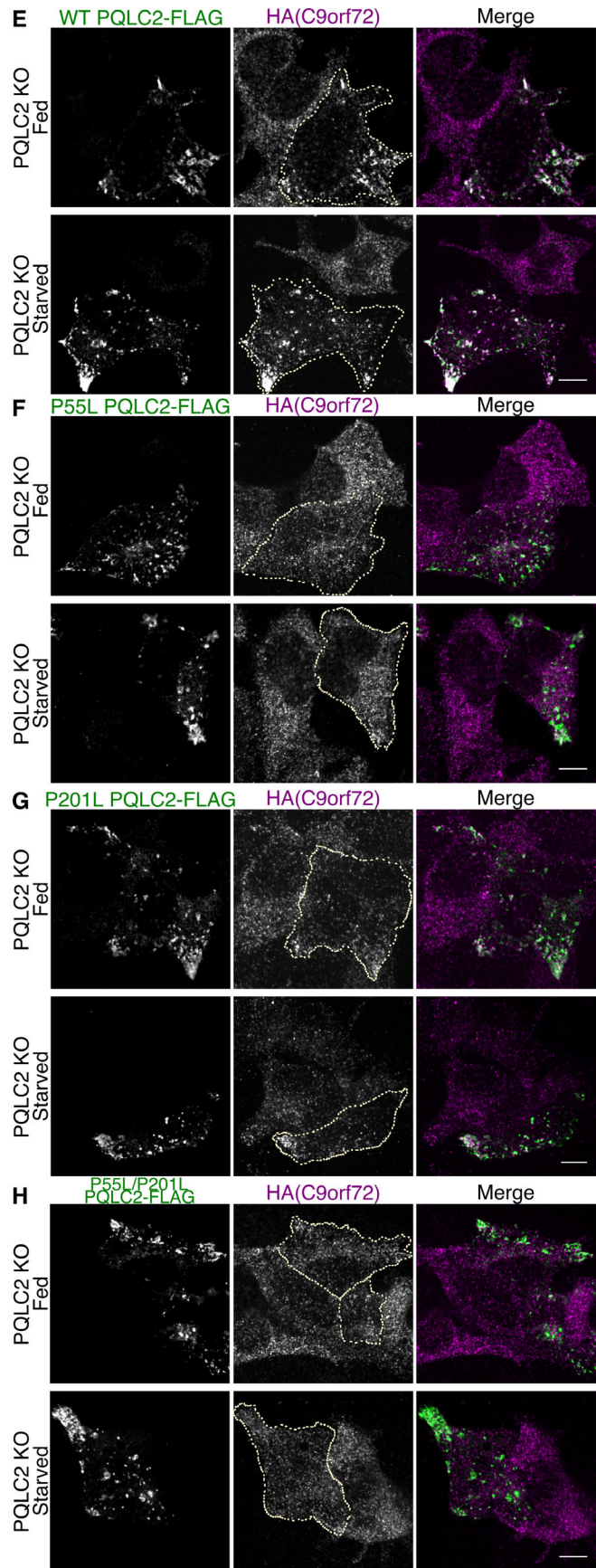
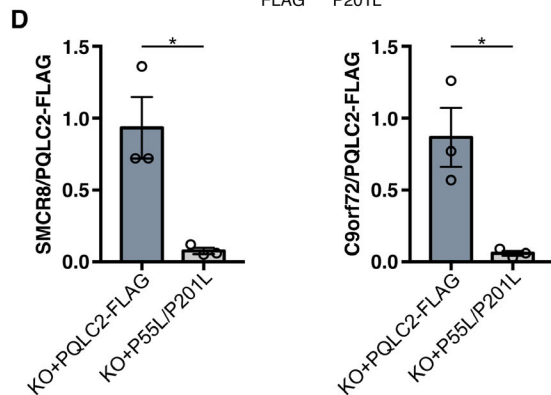
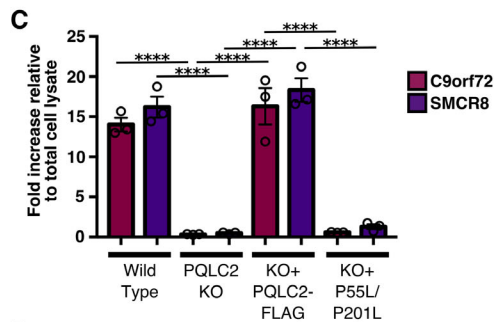
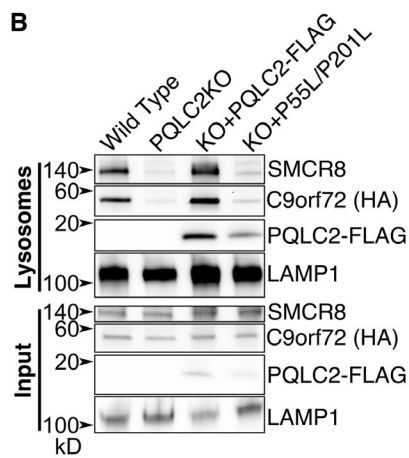
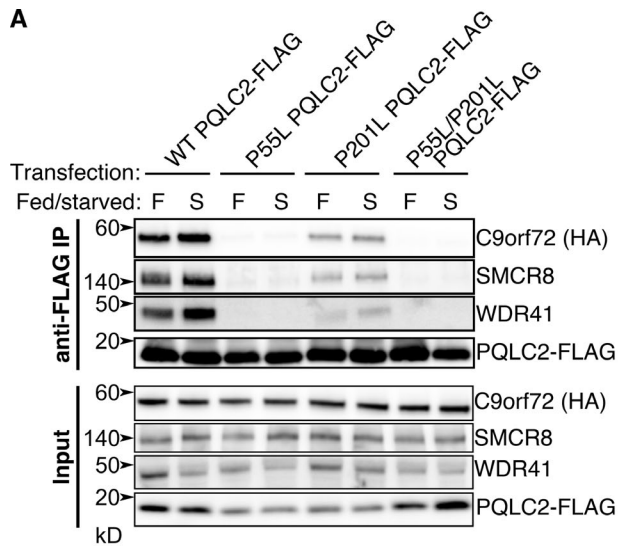


**Figure 3. PQ motif mutations in PQLC2 disrupt C9orf72 complex interactions and recruitment of C9orf72 to lysosomes.** (A) PQLC2 KO cells were transfected with WT PQLC2-FLAG or the indicated mutants. Cells were cultured under fed (F) or starved (S) conditions; PQLC2-FLAG was immunoprecipitated, followed by immunoblotting for FLAG and the endogenous WDR41, C9orf72, and SMCR8 proteins. (B) Iron-dextran-loaded lysosomes were magnetically purified from the parental HEK293FT cells, PQLC2 KO cells, and PQLC2 KO cells stably expressing WT PQLC2-FLAG or P55L/P201L PQLC2-FLAG. Immunoblots are shown of the indicated proteins in the total cell lysate (input) and in magnetically isolated lysosomes (lysosomes). (C) Quantification of immunoblots for the indicated proteins expressed as a fold increase in the lysosome fraction relative to the input (mean  $\pm$  SEM, three independent experiments, data points from individual experiments shown as open circles; \*\*\*\*,  $P \leq 0.0001$ ; ANOVA with Tukey's multiple comparisons test). (D) Lysosomal levels of SMCR8 or C9orf72 normalized to the respective lysosomal PQLC2-FLAG in KO cells expressing WT and mutant PQLC2. Mean  $\pm$  SEM, unpaired *t* test; \*,  $P \leq 0.05$ ,  $n = 3$ . (E–H) PQLC2 KO cells were transfected with WT PQLC2-FLAG or the indicated mutants and cultured in normal growth medium (fed) or amino acid/serum-free RPMI (starved). Cells were fixed and immunostained with FLAG and HA antibodies to examine C9orf72 localization. Transfected cells are outlined with dashed lines. Scale bars: 10  $\mu$ m.

significantly alter this interaction. Therefore, availability of the cationic amino acid substrates of PQLC2 (arginine, lysine, and histidine) specifically regulates the interaction between PQLC2 and components of the C9orf72 complex.

Consistent with the analysis of interactions between the C9orf72 complex and PQLC2, immunofluorescence analysis revealed that C9orf72 recruitment to lysosomes was reduced following addition of the complete MEM-amino acid mix to starved

cells and by arginine, lysine, and histidine, but not by the other amino acids in the MEM mixture (Fig. 5). These results suggest that the availability of its substrates directly regulates the ability of PQLC2 to recruit the C9orf72 complex to lysosomes. An alternative possibility is that substrate availability affects the lysosomal localization of PQLC2 itself. However, we did not observe any impact of changes in amino acid availability on the lysosomal localization of PQLC2 (Fig. S5).

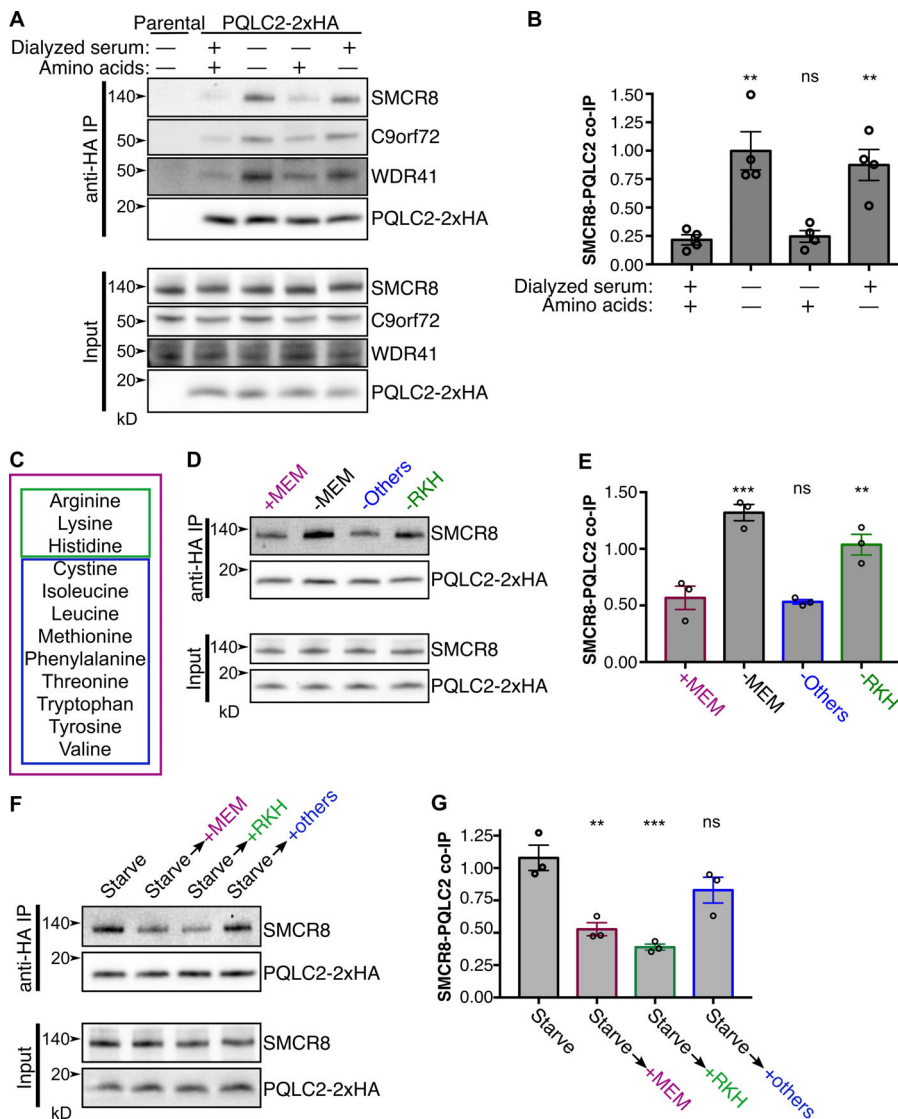


**Figure 4. Amino acid-dependent regulation of the C9orf72 complex's interaction with PQLC2.** (A) WT (parental) or gene-edited cells expressing PQLC2-2xHA from the endogenous locus were incubated in medium with or without amino acids and/or dialyzed serum. PQLC2 was immunoprecipitated, followed by immunoblotting with the indicated antibodies. (B) Summary of the ratio of SMCR8 to PQLC2-2xHA in immunoprecipitations from A. All values are mean  $\pm$  SEM, with data points from individual experiments ( $n = 4$ ) indicated by open circles. \*\*,  $P \leq 0.01$ ; ANOVA with Dunnett's multiple comparisons test. (C) List of amino acids in MEM-amino acid mix. Magenta, green, and blue boxes indicate groups of amino acids used in subsequent experiments. (D) Cells were incubated in media containing the MEM-amino acid mix (+MEM, magenta box), media without amino acids (-MEM), without arginine, lysine, and histidine (-FKH, green box), or without the other amino acids in the MEM mix (-Others, blue box). PQLC2 was then immunoprecipitated to determine the effects of these conditions on the interaction. (E) Summary of the ratio of SMCR8 to PQLC2-2xHA in immunoprecipitations in D. \*\*,  $P \leq 0.01$ ; \*\*\*,  $P \leq 0.001$ ; ANOVA with Dunnett's multiple comparisons test ( $n = 3$ ). (F) Cells were starved and then incubated in media containing the indicated amino acids, followed by immunoprecipitation of PQLC2. (G) Summary of the ratio of SMCR8 to PQLC2-2xHA in immunoprecipitations from F. \*\*,  $P \leq 0.01$ ; \*\*\*,  $P \leq 0.001$ ; ANOVA with Dunnett's multiple comparisons test ( $n = 3$ ).

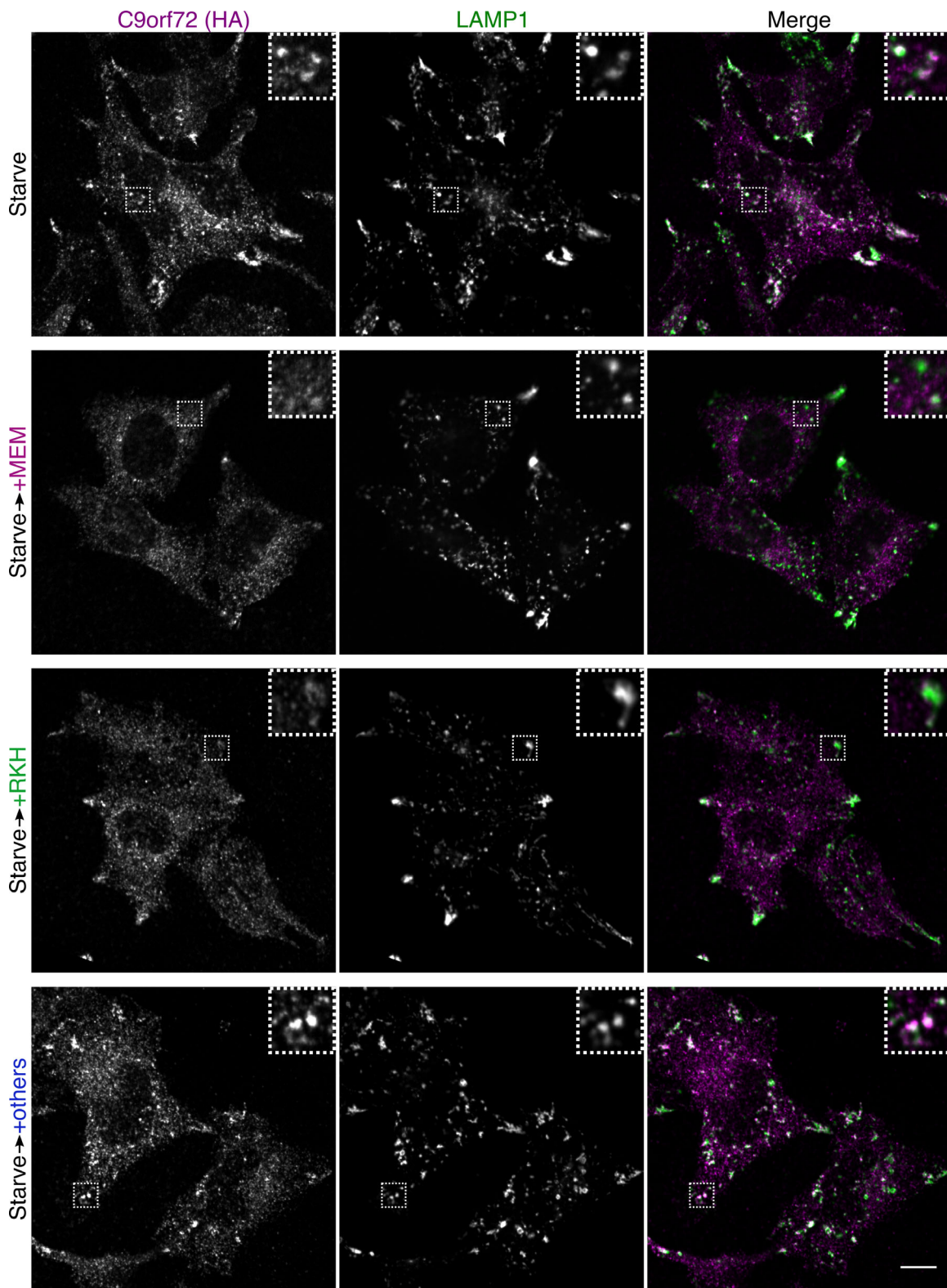


Figure 5. **C9orf72 enrichment on lysosomes is negatively regulated by the availability of cationic amino acids.** Immunofluorescence images of 2xHA-C9orf72 and LAMP1 in cells expressing 2xHA-C9orf72 from the endogenous locus. Cells were starved and then incubated in media containing the indicated amino acids. Scale bar: 10  $\mu$ m. Insets: 7.0  $\mu$ m wide.

The observation that the interaction between the C9orf72 complex and PQLC2 is regulated by availability of the cationic amino acids transported out of lysosomes by PQLC2 suggested that PQLC2 communicates luminal amino acid levels to the C9orf72 complex. To test this model more directly, we designed and implemented a strategy to acutely generate a PQLC2 substrate in the lumen of lysosomes. This took advantage of a known relationship between PQLC2 and cystinosin, the lysosomal transporter for cystine (Kalatzis et al., 2001). Mutations in cystinosin cause cystinosis, a lysosome storage disease characterized by the massive accumulation of cystine within lysosomes (Gahl, 2009; Gahl et al., 1982; Town et al., 1998). Cysteamine is used to treat this disease (Markello et al., 1993; Thoene et al., 1976). It reacts with cystine in lysosomes by sulfhydryl-disulfide exchange to form cysteine and a mixed disulfide (Gahl, 2009; Thoene et al., 1976). This mixed disulfide is structurally similar to lysine and is transported out of lysosomes by PQLC2 (Jézégou et al., 2012; Liu et al., 2012; Pisoni et al., 1985). Thus, adding cysteamine to cystinosin-depleted cells acutely generates a PQLC2 substrate within the lumen of lysosomes (Fig. 6 A).

When WT cells expressing PQLC2-2xHA from the endogenous locus were starved and treated with cysteamine, the interaction between PQLC2 and the C9orf72 complex remained intact. This was expected given that cystinosin prevents the buildup of lysosomal cystine in these cells. However, in a genome-edited cell line that was depleted of cystinosin, acute cysteamine treatment reversed the starvation-induced interaction between PQLC2 and the C9orf72 complex (Fig. 6, B and C). This result supports a model wherein PQLC2 communicates the abundance of its substrates within the lysosome lumen to the cytoplasmic C9orf72 complex.

#### **WDR41 mediates the interaction between the C9orf72 complex and PQLC2**

WDR41 was previously defined as required for the recruitment of C9orf72 and SMCR8 to lysosomes (Amick et al., 2018). We therefore hypothesized that WDR41 would be required for the interaction of the C9orf72 complex with PQLC2. This was tested in WT versus WDR41 KO cells that were transfected with PQLC2-FLAG. PQLC2-FLAG coimmunoprecipitated endogenous WDR41, SMCR8, and C9orf72 in the WT cells, and these interactions between C9orf72, SMCR8, and PQLC2 were abolished in WDR41 KO cells (Fig. 7, A and B). Imaging WDR41 KO cells transfected with PQLC2-FLAG confirmed that PQLC2 still localized robustly to lysosomes in the absence of WDR41 (Fig. 7 C). WT and WDR41 KO cells were next transfected with PQLC2-FLAG, and endogenous C9orf72 localization was examined by immunofluorescence. Although C9orf72 localized to PQLC2-positive lysosomes in WT cells, this pattern of colocalization was absent in WDR41 KOs (Fig. 7 D). Lastly, we asked if WDR41 was able to interact with PQLC2 in the absence of C9orf72 and SMCR8. To this end, WT and C9orf72 + SMCR8 double-KO (DKO) cells were transfected with PQLC2-FLAG. In addition, DKO cells were transfected with FLAG-PAT1 (lysosomal transporter of small neutral amino acids) as a negative control. Subsequent anti-FLAG immunoprecipitation revealed that WDR41 interacted with PQLC2 to a similar extent in both WT and C9orf72 + SMCR8 DKO cells

(Fig. 7, E and F). In contrast, no measurable interaction was observed in these experiments between WDR41 and PAT1-FLAG (negative control). In summary, multiple lines of evidence indicate that WDR41 is critical for the interaction between PQLC2 and the C9orf72 complex at lysosomes.

#### **PQLC2 KO cells exhibit an impaired ability to activate mTORC1 signaling in response to cationic amino acids**

We next investigated the impact of PQLC2 KO on lysosome function. In contrast to a previous study of the *C. elegans* PQLC2 orthologue, which is known as LAAT-1 and is where the loss-of-function mutants exhibited broad defects in lysosomal degradative function (Liu et al., 2012), we did not observe any impairment in the maturation of cathepsins B, D, and L in PQLC2 KO human cells (Fig. 8 A), nor did PQLC2 KO cells accumulate the lipidated form of LC-3 (LC-3 II), a key autophagy protein that is degraded by lysosomes. As a positive control for the ability of this assay to detect lysosome dysfunction, chloroquine treatment (which increases lysosomal pH) dramatically impaired cathepsin maturation and resulted in elevated LC3-II abundance (Fig. 8 A).

In addition to serving a degradative role, lysosomes act as an important signaling hub where the availability of multiple nutrients is sensed and transduced into signals that control the activity of mTORC1. Interestingly, PQLC2 KO cells exhibited a defect in their ability to acutely activate mTORC1 signaling and phosphorylate ribosomal protein S6 kinase (S6K) threonine 389 (T389) in response to cationic amino acids (Fig. 8, B and C). This effect was specifically due to the loss of PQLC2, as reexpression of PQLC2-FLAG in the KO cells rescued phospho-S6K to WT levels in these assays.

The regulation of mTORC1 signaling is complex and dependent on multiple lysosome-localized proteins for coordinating the sensing of amino acid availability with the Rheb-dependent activation of mTORC1 (Angarola and Ferguson, 2019; Wolfson and Sabatini, 2017). To test the contributions of defective PQLC2-dependent C9orf72 complex recruitment to lysosomes to the impaired mTORC1 activation in PQLC2 KO cells, we stably expressed the lysosome targeted C9orf72 chimeric protein in PQLC2 KO cells and measured responsiveness to cationic amino acids. These experiments revealed that reestablishing lysosomal localization of C9orf72 improved the responsiveness of mTORC1 to cationic amino acids in PQLC2 KO cells (Fig. 8, D and E). These results support the functional relevance of the PQLC2-dependent lysosome recruitment mechanism for the C9orf72 complex that we have discovered in this study and form the foundation for future studies into the direct lysosomal functions of the C9orf72 complex.

## **Discussion**

It was previously established that C9orf72 is required for the maintenance of normal lysosome function and is itself part of a protein complex that localizes to the cytoplasmic surface of lysosomes when cells are starved of amino acids (Amick et al., 2016; Corriero and Horvitz, 2018; McAlpine et al., 2018; O'Rourke et al., 2016; Sullivan et al., 2016; Zhang et al., 2018). These observations defined two major questions concerning the

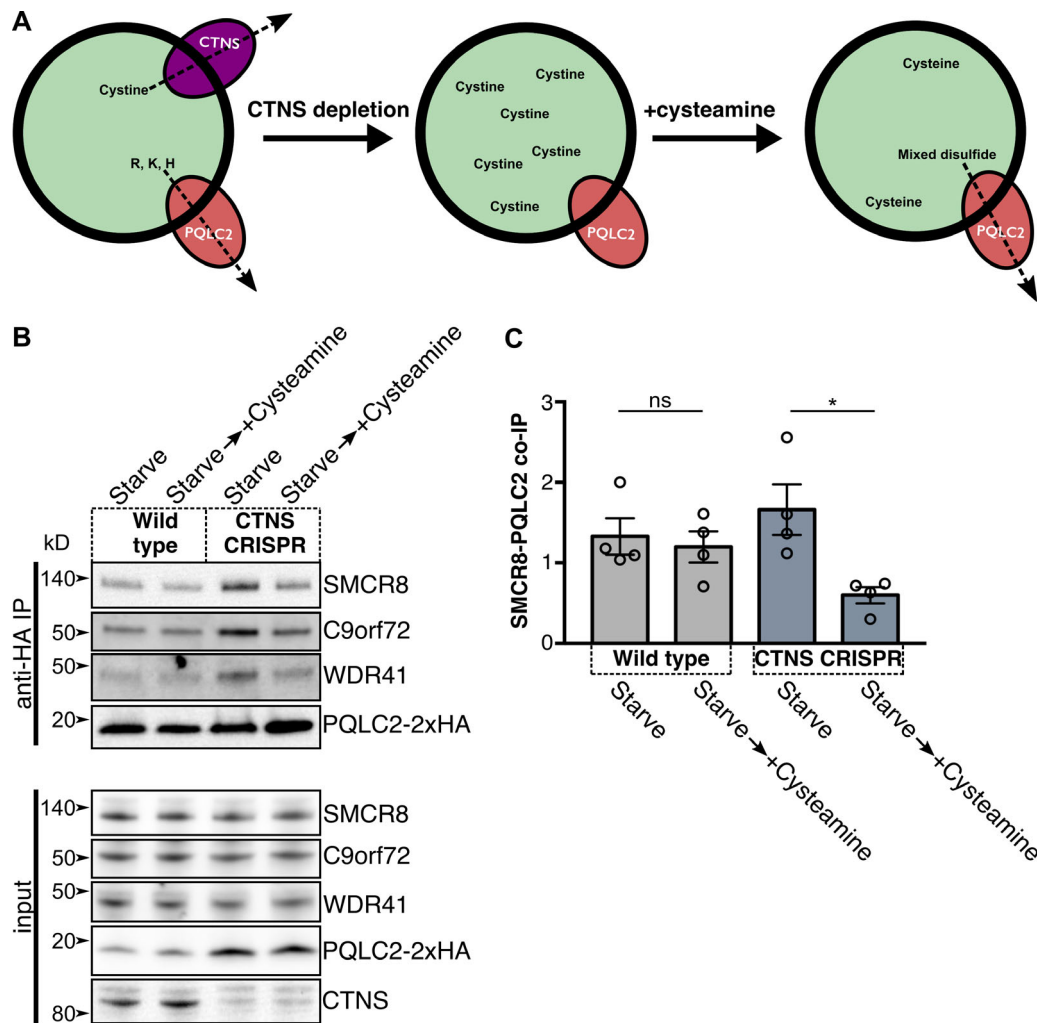


**Figure 6. Lysosomal substrates negatively regulate the interaction between PQLC2 and the C9orf72 complex.** (A) Principle of the cystinosin depletion/cysteamine treatment experiment. Cystinosin (CTNS) is a lysosomal transporter of cystine, and PQLC2 is a lysosomal transporter of arginine, lysine, and histidine. Upon depletion of cystinosin, cystine accumulates within lysosomes. When cysteamine is added, it reacts with cystine in lysosomes to form cysteine and a lysine-like mixed disulfide that can be transported by PQLC2. Therefore, upon cystinosin depletion, a PQLC2 substrate can be acutely generated inside lysosomes by cysteamine addition. (B) WT or cystinosin-depleted cells expressing PQLC2-2xHA from the endogenous locus were starved and then incubated in starvation media containing cysteamine (60 min, 1 mM). PQLC2 was immunoprecipitated from cell lysates, followed by immunoblotting with the indicated antibodies. (C) Summary of the ratio of SMCR8 to PQLC2-2xHA in the immunoprecipitations from B. Values are mean  $\pm$  SEM from four independent experiments with individual data points indicated by open circles; \*,  $P < 0.05$ ; ANOVA with Tukey's multiple comparisons test.

pathway in which C9orf72 functions. First, what is the basis for the regulated interactions that connect the C9orf72 complex to lysosomes? Second, what is the specific function of this complex at lysosomes? In this study, we solved the first of these two problems by identifying a regulated physical interaction between PQLC2, a lysosomal amino acid transporter, and the C9orf72 complex. We furthermore established that PQLC2 is both necessary and sufficient for recruiting the C9orf72 complex to lysosomes. This process is negatively regulated by the cationic amino acids that are transported by PQLC2. We thus identify a new mechanism whereby cationic amino acid availability is sensed at lysosomes. Importantly, this process is distinct from previously defined lysosome-based amino acid-sensing mechanisms that converge on the Rag GTPases for the lysosomal recruitment of mTORC1.

Our results reveal that, in addition to acting as a cationic amino acid transporter, PQLC2 also controls the abundance of

the C9orf72 complex at lysosomes. Other transporters with dual functionality related to substrate transport and signaling have been termed “transceptors” (Holsbeeks et al., 2004). One example of a transceptor is the yeast general amino acid permease (GAP1), which transports a broad range of amino acids and acts as an amino acid sensor that activates protein kinase A signaling (Conrad et al., 2017; Donaton et al., 2003). Meanwhile, at the mammalian lysosome, SLC38A9 is an amino acid transporter that associates with mTORC1 regulatory machinery and communicates the abundance of arginine, lysine, and leucine to this signaling pathway (Jung et al., 2015; Rebsamen et al., 2015; Wang et al., 2015). Another recently reported example of an amino acid transporter with additional functions conferred by an interacting protein is PAT1 (also known as LYAAT-1 and SLC36A1), whose interaction with the PPK-3/PIKfyve lipid kinase is critical for the lysosomal degradation of phagocytic substrates in

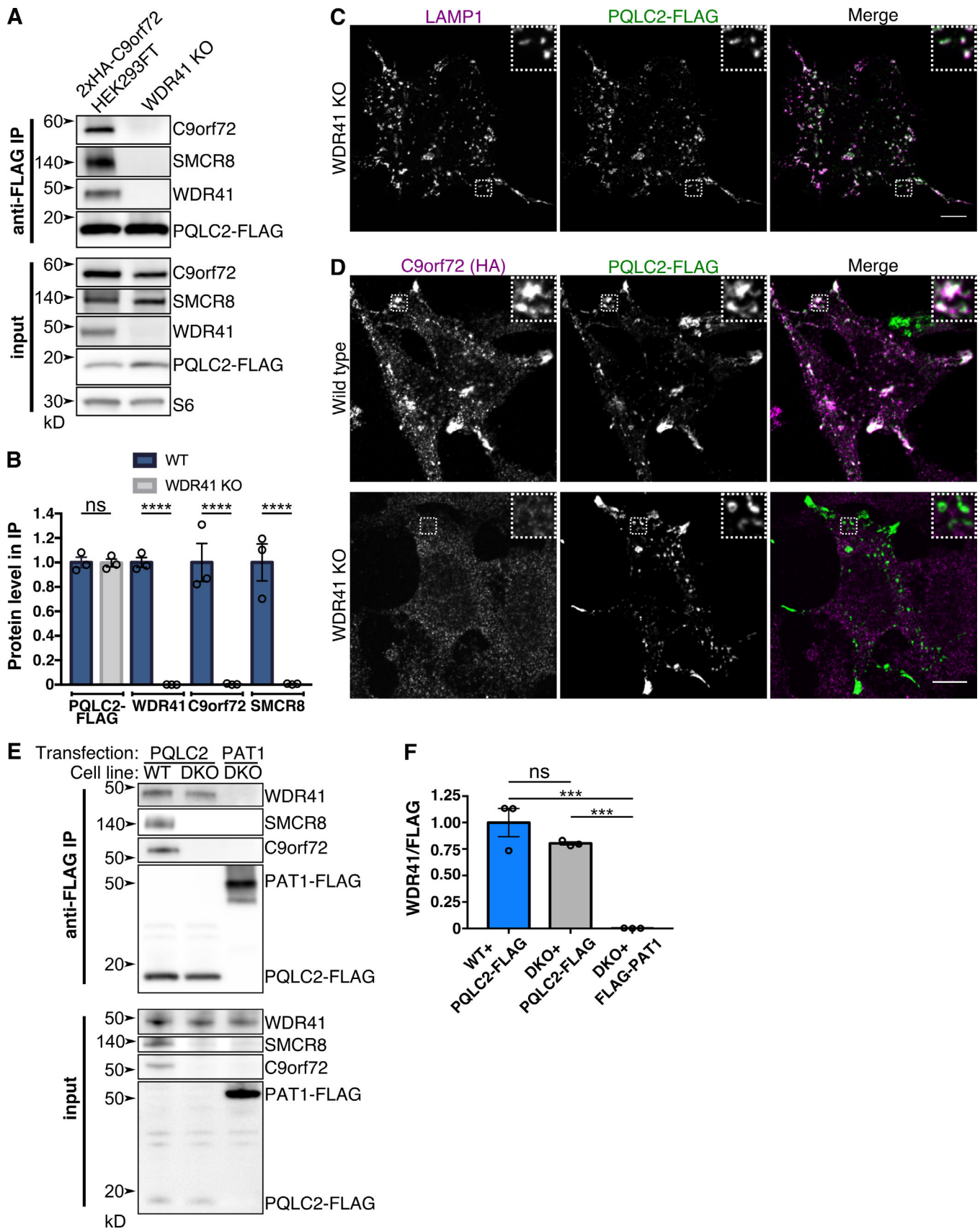


Figure 7. **WDR41 mediates the interaction of the C9orf72 complex with PQLC2.** (A) PQLC2-FLAG was expressed in WT and WDR41 KO cells. Following anti-FLAG immunoprecipitation, PQLC2-FLAG and endogenous WDR41, C9orf72, and SMCR8 were detected by immunoblotting. (B) Summary of results

from A. Levels of the indicated proteins in anti-FLAG immunoprecipitations from WT and WDR41 KO cells (WT levels normalized to 1,  $n = 3$ , mean  $\pm$  SEM plotted with data points from individual experiments [ $n = 3$ ] plotted as open circles; \*\*\*\*,  $P \leq 0.0001$ ). (C) Immunofluorescence of PQLC2-FLAG and LAMP1 in WDR41 KO cells. Scale bar: 10  $\mu$ m. Inset: 6.7  $\mu$ m wide. (D) Immunofluorescence images of C9orf72 localization (endogenously expressed 2xHA-C9orf72) in WT and WDR41 KO cells transiently overexpressing PQLC2-FLAG. Consistent with immunoprecipitation data, overexpression of PQLC2 results in its colocalization with C9orf72 in WT, but not WDR41 KO, cells. Scale bar: 10  $\mu$ m. Insets: 5.0  $\mu$ m wide. (E) WT and C9orf72/SMCR8 DKO were transfected with FLAG-tagged PQLC2 and subjected to anti-FLAG immunoprecipitations. FLAG-tagged PAT1, an unrelated lysosomal amino acid transporter, served as a negative control. (F) Summary of WDR41 levels in anti-FLAG immunoprecipitations from E ( $n = 3$ , mean  $\pm$  SEM plotted with data points from individual experiments plotted as open circles; ANOVA with Tukey's multiple comparisons test; \*\*,  $P \leq 0.001$ ).

*C. elegans* (Gan et al., 2019). Our new data support the inclusion of PQLC2 into the subset of transporters that have the ability to perform a second function.

PQLC2 is part of a family of transporters with distant homology to the bacterial rhodopsin family of receptors, which includes the SWEET/semiSWEET sugar transporters (Xuan et al., 2013; Zhai et al., 2001). Crystal structures of *Escherichia coli* semiSWEET at different steps of its transport cycle revealed that the conserved PQ motif acts as a hinge that allows the transporter to transition between different steps of its transport cycle (Lee et al., 2015). For transceptors, conformational changes that arise during the transport cycle are thought to be transduced to downstream effector proteins (Thevelein and Voordeckers, 2009). The interaction between PQLC2 and the C9orf72 complex is mediated by WDR41 and requires conserved

proline residues within the PQ motifs of PQLC2. This suggests that the interaction between WDR41 and PQLC2 requires conformational changes that are enabled by these hinges in PQLC2, and that mutation of the P55 and P201 residues could therefore lock PQLC2 in a conformation that is unfavorable for its interaction with WDR41. However, the identity of a WDR41 binding site on PQLC2 that is revealed by such conformational changes has not yet been established. An additional possibility for how substrate availability could affect the ability of PQLC2 to interact with WDR41 could be via changes in PQLC2 oligomerization state. Such regulation would parallel reports of the regulation of presynaptic dopamine transporter oligomerization by its substrates (Chen and Reith, 2008). Further progress in this area will require defining the relevant binding sites on PQLC2 and WDR41, insight into structural changes arising in

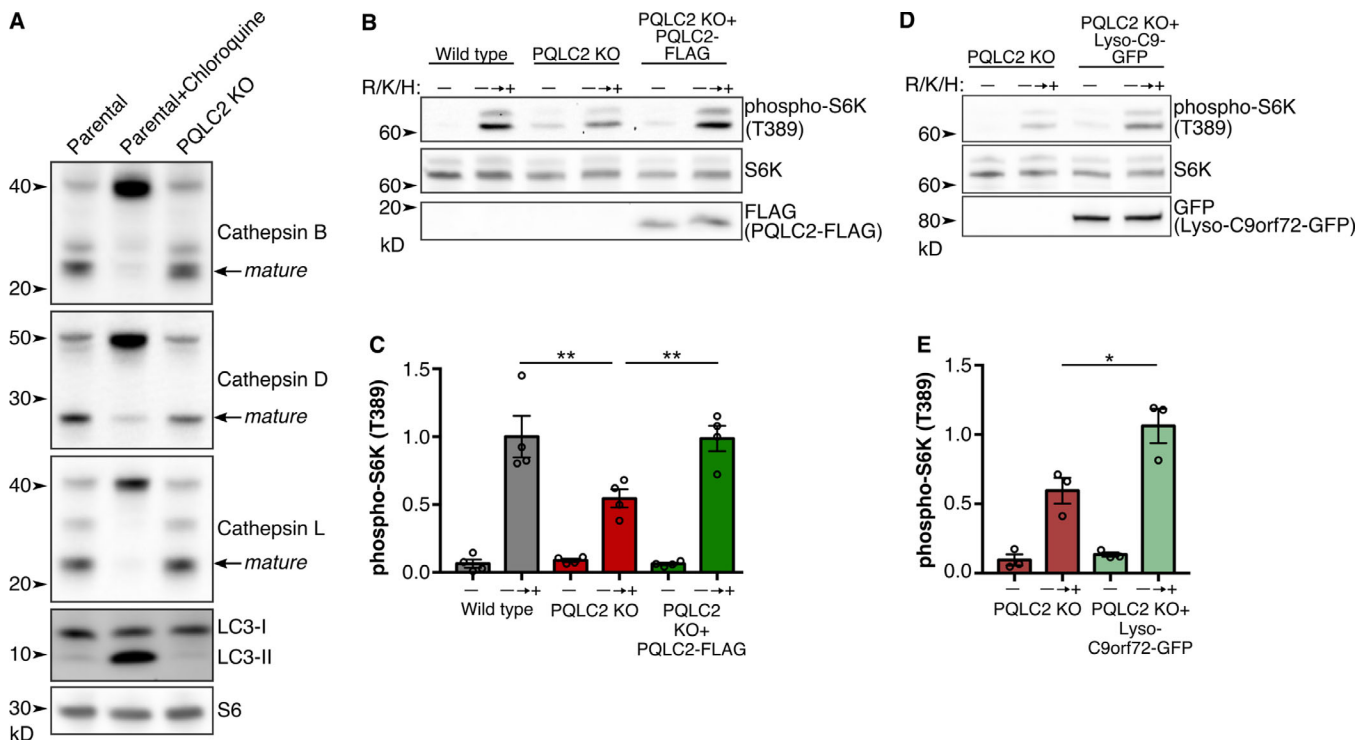


Figure 8. **PQLC2 KO cells exhibit a defect in the activation of mTORC1 by cationic amino acids.** (A) Immunoblot analysis of cathepsin B, D, L, and LC3 in WT and PQLC2 KO cell lines. Ribosomal protein S6 was used as a loading control. WT cells treated with chloroquine (50  $\mu$ M, 15 h) were used as a positive control of impaired lysosome function. (B) Immunoblot analysis of S6K T389 phosphorylation levels during starvation for arginine, lysine, and histidine (R/K/H) and upon subsequent R/K/H refeeding in WT, PQLC2 KO, and in KO cells stably expressing PQLC2-FLAG. (C) Quantification of phospho-S6K levels in the indicated conditions in B (normalized to total S6K levels; mean  $\pm$  SEM with data points from individual experiments [ $n = 4$ ] indicated by open circles; \*\*,  $P \leq 0.01$ ; ANOVA with Tukey's multiple comparisons test). (D) Immunoblot analysis of phospho-S6K levels during starvation for R/K/H and subsequent R/K/H refeeding in PQLC2 KO and in PQLC2 KO cells stably expressing lysosome-targeted C9orf72-GFP. (E) Quantification of phospho-S6K levels in the indicated conditions in D (\*,  $P < 0.05$ ; ANOVA with Tukey's multiple comparisons test,  $n = 3$ ).

PQLC2 during its transport cycle, and knowing how the presence or absence of amino acid substrates in the lysosome lumen and/or cytosol alter these states.

We used cystinosis depletion combined with cysteamine treatment as a tool to acutely generate a PQLC2 substrate within the lysosome lumen as a strategy to test the effect of lysosomal substrate on the interaction between PQLC2 and the C9orf72 complex. The observation that this treatment negatively regulates the PQLC2–C9orf72 complex interaction also reveals a potential unanticipated effect of cysteamine treatment, which could merit investigation in the context of cystinosis disease therapy (Markello et al., 1993).

Like the C9orf72 complex, the FLCN–FNIP heterodimer also preferentially associates with lysosomes in response to amino acid depletion (Meng and Ferguson, 2018; Petit et al., 2013; Tsun et al., 2013). The FLCN–FNIP and the C9orf72 complexes both contain two interacting DENN (differentially expressed in normal and neoplastic cells) domain proteins (Amick and Ferguson, 2017). However, these two complexes possess distinct mechanisms underlying their regulation. While FLCN–FNIP is recruited to lysosomes via a direct interaction with Rag GTPases (Meng and Ferguson, 2018; Petit et al., 2013; Tsun et al., 2013), the C9orf72 complex instead relies on the interaction between WDR41 and PQLC2. The interaction between FLCN–FNIP and the Rags is selective for the GDP-bound state of RagA/B and is thus dependent on GATOR1, the GAP that stimulates RagA/B GTPase activity (Bar-Peled et al., 2013; Meng and Ferguson, 2018). The specificity of these unique mechanisms for responding to changes in amino acid availability is illustrated by our observations that FLCN is still enriched on lysosomes following the starvation of PQLC2 KO cells (Fig. 2 D) and the intact recruitment of C9orf72 to lysosomes in NPRL3 (GATOR1 subunit) KO cells (Fig. S2 C). These results demonstrate that interactions between the C9orf72 complex and PQLC2 define a distinct amino acid-sensing pathway at the lysosome.

Both the C9orf72 and SMCR8 proteins are predicted to contain DENN domains (Levine et al., 2013; Zhang et al., 2012). In other proteins, DENN domains are best characterized for their role as guanine nucleotide exchange factors for small GTPases of the Rab family (Marat et al., 2011; Wu et al., 2011). However, although several small GTPases have been proposed to function with the C9orf72 complex, including Rab1 (Webster et al., 2016), Rab3 (Frick et al., 2018), Rab5 (Shi et al., 2018), Rab8 and Rab39 (Sellier et al., 2016), and Arf6 (Sivadasan et al., 2016), none of them are known to have lysosome-localized functions that are regulated by either C9orf72 or SMCR8. Our new identification of a PQLC2-dependent mechanism that explains how the C9orf72 complex is recruited to lysosomes provides a foundation for future efforts to identify the downstream targets of the C9orf72 complex at lysosomes and to integrate this pathway into a broader understanding of how nutrient sensing at lysosomes is integrated into the control of cellular physiology.

In summary, we have identified the cationic amino acid transporter PQLC2 as a lysosome-localized binding partner for the C9orf72 complex that is essential for the recruitment of C9orf72, SMCR8, and WDR41 to lysosomes when cells are deprived of cationic amino acids. Our results furthermore suggest

that conformational changes induced by the availability of luminal substrates are critical for the regulated interactions between PQLC2 and the C9orf72 complex. Collectively, these new findings reveal the existence of a mechanism whereby cationic amino acid levels in the lysosome lumen are sensed and transduced into a signal that is initiated by the recruitment of the C9orf72 complex to the cytoplasmic surface of lysosomes.

## Materials and methods

### Cell culture and transfection

HEK293FT cells (Life Technologies) were grown in DMEM + 4.5 g/liter D-glucose, L-glutamine (Gibco), 10% FBS, and 1% penicillin/streptomycin supplement (Mediatech). Transfections were performed with 4 µg DNA, 800 µl OptiMEM (Invitrogen), and 12 µl FuGENE 6 transfection reagent (Promega) per 10-cm dish. Cells were analyzed 2 d after transfection. In experiments examining cathepsin maturation and LC-3 clearance, cells were incubated with 50 µM chloroquine (Sigma-Aldrich) for 15 h.

### Plasmids

PQLC2-FLAG plasmids were generated as follows. The PQLC2 coding sequence was purchased as a gBlock (Integrated DNA Technologies). The gBlock sequence is listed in dataset 1. This DNA was inserted into SmaI-digested pEGFPN2 vector (Clontech) by Gibson Assembly (NEBuilder HiFi DNA Assembly; New England BioLabs) according to manufacturer protocols. A FLAG tag (DYKDDDDK tag) followed by a stop codon was then inserted using the Q5 Site-Directed Mutagenesis Kit (New England BioLabs) according to manufacturer protocols. Primers for this reaction are listed in Table S1. PQLC2 mutants were also generated using the Q5 Site-Directed Mutagenesis Kit, and primers for generating these mutants are listed in Table S1. For lentivirus-mediated transgenic expression of PQLC2-FLAG and mutants, these sequences were amplified by PCR from plasmids described above and inserted into SmaI-digested pLVX-puro vector (Clontech) by Gibson Assembly. The PAT1/SLC36A1 cDNA was amplified by PCR, digested with HindIII and XhoI restriction enzymes, and cloned into the corresponding sites in the pcDNA5/FTR/TO plasmid (Invitrogen). Sequences for the PCR primers used above are provided in Table S1. Generation of the Lyso–C9orf72–GFP plasmid and the SMCR8–tdTomato plasmid was described previously (Amick et al., 2016, 2018). Stbl3 *E. coli* (Invitrogen) was used for cloning pLVX-puro plasmids and XL1-Blue *E. coli* (Agilent) was used for cloning other plasmids. All plasmids were sequence verified. FLAG pLJM1 RagB and RagD plasmids were provided by David Sabatini (Massachusetts Institute of Technology, Cambridge, MA; Addgene plasmids 19313 and 19316; Sancak et al., 2008).

### Immunoprecipitation and immunoblotting

Prior to plating cells, 10-cm dishes were coated with 2 µg/ml Poly-D-lysine (Sigma-Aldrich) in PBS overnight and then washed twice with PBS. Prior to lysis, dishes were washed with ice-cold PBS. Cells were then lysed in 50 mM Tris, pH 7.4, 150 mM NaCl, 1 mM EDTA, and 1% Triton X-100 plus protease and phosphatase inhibitor cocktails (Complete Mini, EDTA-free,

PhosSTOP). Insoluble material was cleared by centrifugation for 10 min at 20,000  $\times g$ . Immunoprecipitations were performed on the resulting lysates. For anti-HA immunoprecipitations, anti-HA Affinity Matrix (Roche Diagnostics) was used. For anti-FLAG immunoprecipitations, anti-FLAG M2 affinity gel was used (Sigma-Aldrich). Lysates were added to resin and incubated for 1 h at 4°C with rotation. Afterwards, resin was washed five times with lysis buffer and then eluted with 2 $\times$  Laemmli buffer at 50°C for 3 min. Laemmli buffer was removed from resin and 6.25% 2-mercaptoethanol was added. Immunoblotting was performed with 4–15% gradient Mini-PROTEAN TGX precast polyacrylamide gels and nitrocellulose membranes (Bio-Rad). Blots were blocked with 5% nonfat dry milk (AmericanBIO), and antibodies were incubated with 5% nonfat dry milk or BSA (AmericanBIO) in TBS with 0.1% Tween 20. Chemiluminescence detection of HRP signals from secondary antibodies was performed on a Versa-Doc imaging station (Bio-Rad). Antibodies used in this study are listed in Table S2.

## MS

HeLa cells expressing Lyso-C9orf72-GFP and SMCR8-tdTomato or Lyso-GFP and SMCR8-tdTomato were lysed as described above. Lysates were incubated with GFP-Trap resin (Chromotek) for 2 h at 4°C. After washing in lysis buffer, bound proteins were eluted with 2 $\times$  Laemmli buffer and heated at 37°C. Samples were then run ~10 mm into an SDS-PAGE gel, silver stained, and excised from the gel.

Silver-stained gel bands were treated with 5% acetic acid for 10 min with rocking. The acid was removed and the bands were covered with freshly prepared destaining solution (1:1 ratio of stock solutions of 30 mM potassium ferricyanide in water and 100 mM sodium thiosulfate in water) until the brownish color disappeared. The bands were then rinsed three times with 0.5 ml water for 5 min to remove the acid and chemical reducing agents. The gel bands were cut into small pieces and washed for 30 min on a tilt table with 450  $\mu$ l of 50% acetonitrile/100 mM  $\text{NH}_4\text{HCO}_3$ , followed by a 30-min wash with 50% acetonitrile/12.5 mM  $\text{NH}_4\text{HCO}_3$ . The gel bands were shrunk by the brief addition and subsequent removal of acetonitrile and then dried by speed vacuum. Each sample was resuspended in 100  $\mu$ l of 25 mM  $\text{NH}_4\text{HCO}_3$  containing 0.5  $\mu$ g of digestion-grade trypsin (V5111; Promega) and incubated at 37°C for 16 h. Supernatants containing tryptic peptides were transferred to new Eppendorf tubes, and the gel bands were extracted with 300  $\mu$ l of 80% acetonitrile/0.1% trifluoroacetic acid for 15 min. Supernatants were combined and dried by speed vacuum. Peptides were dissolved in 24  $\mu$ l MS loading buffer (2% acetonitrile and 0.2% trifluoroacetic acid), with 5  $\mu$ l injected for liquid chromatography–MS/MS (LC–MS/MS) analysis.

LC–MS/MS analysis was performed on a Thermo Fisher Scientific Q Exactive Plus equipped with a Waters NanoACQUITY ultra performance liquid chromatography system using a binary solvent system (A: 100% water, 0.1% formic acid; B: 100% acetonitrile, 0.1% formic acid). Trapping was performed at 5  $\mu$ l/min, 97% buffer A for 3 min using a Waters Symmetry C18 180  $\mu$ m  $\times$  20 mm trap column. Peptides were separated using an ACQUITY ultra performance liquid chromatography PST (BEH) C18 nanoACQUITY Column 1.7  $\mu$ m, 75  $\mu$ m  $\times$  250 mm (37°C) and

eluted at 300 nl/min with the following gradient: 3% buffer B at initial conditions, 5% B at 1 min, 35% B at 90 min, 50% B at 105 min, 90% B at 110 min, 90% B at 115 min, and returned to initial conditions at 116 min. MS was acquired in profile mode over the 300–1,700 m/z range using one microscan, 70,000 resolution, automatic gain control target of 3E6, and a maximum injection time of 45 ms. Data-dependent MS/MS were acquired in centroid mode on the top 20 precursors per MS scan using one microscan, 17,500 resolution, automatic gain control target of 1E5, maximum injection time of 100 ms, and an isolation window of 1.7 m/z. Precursors were fragmented by higher-energy C-trap dissociation activation with a collision energy of 28%. MS/MS were collected on species with an intensity threshold of 2E4, charge states 2–6, and peptide match preferred. Dynamic exclusion was set to 20 s.

Tandem mass spectra were extracted by Proteome Discoverer software (version 2.2.0.388; Thermo Fisher Scientific) and searched in-house using the Mascot algorithm (version 2.6.0; Matrix Science). The data were searched against the SwissProt database (version 2017\_09) with taxonomy restricted to *Homo sapiens* (20,238 sequences). Search parameters included trypsin digestion with up to two missed cleavages, peptide mass tolerance of 10 ppm, MS/MS fragment tolerance of 0.02 D, and methionine oxidation as a variable modification. Normal and decoy database searches were run, with the confidence level set to 95% ( $P < 0.05$ ). Scaffold (version Scaffold 4.8.9; Proteome Software) was used to validate and compare MS/MS-based peptide and protein identifications.

## Immunofluorescence and microscopy

A Nikon Inverted Eclipse TI-E Microscope equipped with 60 $\times$  chromatic aberration-free infinity (CFI) Plan Apo violet correction, NA 1.4, oil immersion and 40 $\times$  CFI Plan Apo, NA 1.0, oil immersion objectives, a spinning-disk confocal-scan head (CSU-X1; Yokogawa), and Volocity software (PerkinElmer) were used for spinning-disk confocal microscopy. Images were acquired at room temperature (22°C). Cells were grown on 12-mm No. 1.5 coverslips (Carolina Biological Supply) coated with Poly-D-lysine (Sigma-Aldrich) and fibronectin (EMD-Millipore). Cells were fixed by adding 1 vol of 8% PFA in 0.1 M sodium phosphate to the culture media in a dropwise manner. Cells were fixed at room temperature for 30 min and then washed with PBS. Samples were permeabilized by immersing coverslips in ice-cold methanol for 3 s, followed by PBS rinses. Samples were then blocked in 5% normal donkey serum (Jackson ImmunoResearch)/PBS for 1 h at room temperature. All subsequent antibody incubations were performed in this buffer. Antibodies used in this study are listed in Table S2. The protocol for detecting 2xHA-tagged endogenously expressed protein was performed as described previously (Petit et al., 2013). The percentage of starved cells with C9orf72 puncta colocalized with LAMP1 in Fig. 2 was made by visual inspection of images from three independent experiments with >140 cells per cell line analyzed. Images were processed with ImageJ/FIJI (Schindelin et al., 2012). For analysis of protein colocalization, Pearson's correlation was determined with Cell Profiler (McQuin et al., 2018).

### CRISPR/Cas9 genome editing

gRNA targeting exon 2 of *PQLC2* and exon 3 of *CTNS* (the gene encoding cystinosin) were selected from predesigned gRNA sequences (Wang et al., 2014). Cloning of gRNA-encoding DNA oligonucleotides (Integrated DNA Technologies) into Bbs1-digested pX459 vector was done as described previously (Amick et al., 2018; Ran et al., 2013). Oligonucleotide sequences for generating the gRNA used to target *PQLC2* and *CTNS* are listed in Table S1. Sequences of the gRNA plasmids were confirmed by sequencing. Nprl3 gRNA sequences are described elsewhere (Meng and Ferguson, 2018). 0.4 µg plasmid DNA was transfected with FuGENE 6 into 250,000 cells in a 6-well dish. The next day, transfected cells were selected with 1.25 µg/ml puromycin for 3 d. Surviving cells were subsequently plated at clonal density. Following the selection and expansion of colonies, *PQLC2* KO cells were identified by sequencing of PCR-amplified genomic DNA. To sequence genomic DNA, it was extracted (QuickExtract DNA extraction solution; Epicentre Biotechnologies), and the region of interest was amplified by PCR (primers described in Table S3), cloned into the pCR-Blunt TOPO vector (Zero Blunt TOPO PCR cloning kit; Thermo Fisher Scientific), and transformed into TOP10-competent *E. coli* cells. Plasmid DNA was then isolated from colonies and sequenced to define the genotype of the locus of interest.

The method used for CRISPR/Cas9 genome editing to insert epitope tags at endogenous loci was described previously (Amick et al., 2018). The single-strand DNA oligonucleotide homology-directed repair donor template was designed with asymmetric homology arms on the protospacer-adjacent motif proximal and distal sides of the cut site in order to enhance the efficiency of tag insertion (Richardson et al., 2016). The single-strand DNA oligonucleotide repair template and protospacer sequences (Integrated DNA Technologies) used to insert the 2xHA epitope tag into the *PQLC2* gene are listed in Table S4. Clonal cell populations were isolated and screened for HA signal by immunoblotting and immunofluorescence. To further confirm the correct in-frame insertion of the 2xHA tag in these cells, genomic DNA surrounding the site of tag insertion was PCR amplified and sequenced as described above. Primer sequences used for this purpose are listed in Table S3.

### Magnetic isolation of lysosomes

Magnetic isolation of lysosomes from cells that were endocytically loaded with colloidal iron dextran nanoparticles was performed as described previously (Amick et al., 2018). Lysosomes were purified from the following cell lines under starved conditions: HEK293FT cells expressing 2xHA-C9orf72 from the endogenous locus, *PQLC2* KO in the background of the aforementioned cell line, *PQLC2* KO cells stably expressing WT *PQLC2*-FLAG, and cells stably expressing P55L/P201L *PQLC2*-FLAG. Lentiviral transduction was used to achieve stable transgenic expression of *PQLC2*-FLAG and P55L/P201L mutant. Generation of plasmids for this purpose is described above. Lentivirus packaging and infection was performed as described previously (Amick et al., 2018).

### Amino acid starvation and refeeding

For cells analyzed in fed conditions, cells were incubated with fresh normal growth media (DMEM) as described above for 2 h before

analysis. For starvation experiments, dishes were washed with PBS and then incubated in RPMI medium without amino acids, without serum, and with glucose (United States Biological). Where indicated, dialyzed FBS was added to this media (Gibco). Also where indicated, MEM-amino acids solution (Gibco) was added to this media. For experiments in Fig. 4 A, cells were incubated in media with or without these components for 2 h before lysis. The MEM-amino acids solution at 1× contains L-arginine (600 µM), L-cystine (100 µM), L-histidine (200 µM), L-isoleucine (400 µM), L-leucine (400 µM), L-lysine (396 µM), L-methionine (101 µM), L-phenylalanine (200 µM), L-threonine (400 µM), L-tryptophan (50 µM), L-tyrosine (199 µM), and L-valine (400 µM). Mixtures of individual amino acids were prepared to yield the “RKH” and “other” amino acids at their respective concentrations. For experiments in Fig. 4 F, cells were incubated in starvation media for 2 h, followed by incubation in media containing the indicated groups of amino acids for 1 h. For experiments in Fig. 4 D, cells were incubated in media lacking the indicated amino acids and containing the others at their respective concentrations in the MEM-amino acids solution.

For studies of mTORC1 activation by cationic amino acids in *PQLC2* KO cells, dishes were washed with PBS, and then cells were starved for 2 h by incubation with RPMI medium without serum, with glucose, and with 1× cystine, isoleucine, leucine, methionine, phenylalanine, threonine, tryptophan, tyrosine, and valine. Amino acid refeeding was performed by addition of 1× arginine, lysine, and histidine to this media and incubation with cells for 15 min.

### Cystinosin depletion and cysteamine treatment

gRNAs used to target the *CTNS* gene and the method of generating a cystinosin-depleted clonal cell line in the background of *PQLC2*-2xHA cells is described in the CRISPR/Cas9 genome editing section and Table S1. These cells (and the parental *PQLC2*-2xHA cell line) were starved as described above, and then cysteamine (Sigma-Aldrich) was added to starvation media at 1 mM final concentration for 1 h before lysis. Immunoprecipitations and immunoblotting were performed as described in previous sections.

### Statistical analysis

Data were analyzed using Prism (GraphPad software), and specific statistical tests are specified in the figure legends. All error bars represent SEM. Data distribution was assumed to be normal, but this was not formally tested.

### Online supplemental material

Fig. S1 shows the localization of FLAG-tagged *PQLC2* and PAT1. Fig. S2 shows the localization of C9orf72 in GATOR1-deficient cells. Fig. S3 shows the subcellular localization of *PQLC2* mutants. Fig. S4 shows the 2xHA epitope tagging of the endogenous *PQLC2*. Fig. S5 shows the localization of *PQLC2* under different nutrient conditions. Table S1 contains DNA sequences used for generating the plasmids used in this study. Table S2 contains the antibodies used in this study. Table S3 contains the primers used for PCR amplification of genomic DNA. Table S4 contains the sequences used for the *PQLC2* CRISPR knockin. Dataset

1 contains the gBlock sequence used to generate the PQLC2-FLAG plasmid.

## Acknowledgments

We appreciate the laboratory management efforts, technical expertise, and insightful comments from Agnes Ferguson that supported this project, and are grateful to all members of the Ferguson laboratory for helpful advice and discussion. We thank Jean Kanyo of the Mass Spectrometry and Proteomics Resource of the W.M. Keck Foundation Biotechnology Resource Laboratory at Yale University for her work on MS experiments.

MS experiments were supported by National Institutes of Health shared-instrument grant 1S10OD018034-01. This research was supported by National Institutes of Health grant GM105718 to S.M. Ferguson. J. Amick was supported by National Institutes of Health grants T32GM007223 and F31GM119249.

The authors declare no competing financial interests.

Author contributions: J. Amick helped write the manuscript and led efforts related to experiment design, performing experiments, data analysis, and figure preparation. A.K. Tharkeshwar conducted experiments related to lysosome purification. G. Talaia performed experiments relating to investigating the interaction between the C9orf72 complex and PQLC2. S.M. Ferguson supervised the project, designed experiments, analyzed the data, and led the writing of the manuscript. Through ongoing discussion of results, all authors contributed to the overall direction of the project.

Submitted: 13 June 2019

Revised: 7 October 2019

Accepted: 25 October 2019

## References

- Amick, J., and S.M. Ferguson. 2017. C9orf72: At the intersection of lysosome cell biology and neurodegenerative disease. *Traffic*. 18:267–276. <https://doi.org/10.1111/tra.12477>
- Amick, J., A. Rocznik-Ferguson, and S.M. Ferguson. 2016. C9orf72 binds SMCR8, localizes to lysosomes, and regulates mTORC1 signaling. *Mol. Biol. Cell*. 27:3040–3051. <https://doi.org/10.1091/mbc.e16-01-0003>
- Amick, J., A.K. Tharkeshwar, C. Amaya, and S.M. Ferguson. 2018. WDR41 Supports Lysosomal Response to Changes in Amino Acid Availability. *Mol. Biol. Cell*. 29:2213–2227. <https://doi.org/10.1091/mbc.E17-12-0703>
- Angarola, B., and S.M. Ferguson. 2019. Weak membrane interactions allow rheb to activate mTORC1 signaling without major lysosome enrichment. *Mol. Biol. Cell*. 30:2750–2760. <https://doi.org/10.1091/mbc.E19-03-0146>
- Bar-Peled, L., and D.M. Sabatini. 2014. Regulation of mTORC1 by amino acids. *Trends Cell Biol*. 24:400–406. <https://doi.org/10.1016/j.tcb.2014.03.003>
- Bar-Peled, L., L. Chantranupong, A.D. Cherniack, W.W. Chen, K.A. Ottina, B.C. Grabiner, E.D. Spear, S.L. Carter, M. Meyerson, and D.M. Sabatini. 2013. A Tumor suppressor complex with GAP activity for the Rag GTPases that signal amino acid sufficiency to mTORC1. *Science*. 340:1100–1106. <https://doi.org/10.1126/science.1232044>
- Belzil, V.V., P.O. Bauer, M. Prudencio, T.F. Gendron, C.T. Stetler, I.K. Yan, L. Pregent, L. Daugherty, M.C. Baker, R. Rademakers, et al. 2013. Reduced C9orf72 gene expression in c9FTD/ALS is caused by histone trimethylation, an epigenetic event detectable in blood. *Acta Neuropathol*. 126:895–905. <https://doi.org/10.1007/s00401-013-1199-1>
- Chen, N., and M.E. Reith. 2008. Substrates dissociate dopamine transporter oligomers. *J. Neurochem*. 105:910–920. <https://doi.org/10.1111/j.1471-4159.2007.05195.x>
- Conrad, M., H.N. Kankipati, M. Kimpe, G. Van Zeebroeck, Z. Zhang, and J.M. Thevelein. 2017. The nutrient transceptor/PKA pathway functions independently of TOR and responds to leucine and Gcn2 in a TOR-

- independent manner. *FEMS Yeast Res*. 17:17. <https://doi.org/10.1093/femsyr/fox048>
- Corrionero, A., and H.R. Horvitz. 2018. A C9orf72 ALS/FTD Ortholog Acts in Endolysosomal Degradation and Lysosomal Homeostasis. *Curr. Biol*. 28:1522–1535.e5. <https://doi.org/10.1016/j.cub.2018.03.063>
- DeJesus-Hernandez, M., I.R. Mackenzie, B.F. Boeve, A.L. Boxer, M. Baker, N.J. Rutherford, A.M. Nicholson, N.A. Finch, H. Flynn, J. Adamson, et al. 2011. Expanded GGGGCC hexanucleotide repeat in noncoding region of C9ORF72 causes chromosome 9p-linked FTD and ALS. *Neuron*. 72:245–256. <https://doi.org/10.1016/j.neuron.2011.09.011>
- Donaton, M.C., I. Holsbeeks, O. Lagatie, G. Van Zeebroeck, M. Crauwels, J. Winderickx, and J.M. Thevelein. 2003. The Gap1 general amino acid permease acts as an amino acid sensor for activation of protein kinase A targets in the yeast *Saccharomyces cerevisiae*. *Mol. Microbiol*. 50:911–929. <https://doi.org/10.1046/j.1365-2958.2003.03732.x>
- Frick, P., C. Sellier, I.R.A. Mackenzie, C.Y. Cheng, J. Tahraoui-Bories, C. Martinat, R.J. Pasterkamp, J. Prudlo, D. Edbauer, M. Oulad-Abdelghani, et al. 2018. Novel antibodies reveal presynaptic localization of C9orf72 protein and reduced protein levels in C9orf72 mutation carriers. *Acta Neuropathol. Commun*. 6:72. <https://doi.org/10.1186/s40478-018-0579-0>
- Gahl, W.A. 2009. Cystinosis. In *Pediatric Nephrology*. Vol. Sixth. E. Avner, W. Harmon, P. Niaudet, and N. Yoshikawa, editors. Springer, Berlin. 1019–1038. [https://doi.org/10.1007/978-3-540-76341-3\\_41](https://doi.org/10.1007/978-3-540-76341-3_41)
- Gahl, W.A., N. Bashan, F. Tietze, I. Bernardini, and J.D. Schulman. 1982. Cystine transport is defective in isolated leukocyte lysosomes from patients with cystinosis. *Science*. 217:1263–1265. <https://doi.org/10.1126/science.7112129>
- Gan, Q., X. Wang, Q. Zhang, Q. Yin, Y. Jian, Y. Liu, N. Xuan, J. Li, J. Zhou, K. Liu, et al. 2019. The amino acid transporter SLC-36.1 cooperates with PtdIns3P 5-kinase to control phagocytic lysosome reformation. *J. Cell Biol*. 218:2619–2637. <https://doi.org/10.1083/jcb.2019101074>
- Gijssels, I., T. Van Langenhove, J. van der Zee, K. Slegers, S. Philtjens, G. Kleinberger, J. Janssens, K. Bettens, C. Van Cauwenbergh, S. Pereson, et al. 2012. A C9orf72 promoter repeat expansion in a Flanders-Belgian cohort with disorders of the frontotemporal lobar degeneration-amyotrophic lateral sclerosis spectrum: a gene identification study. *Lancet Neurol*. 11:54–65. [https://doi.org/10.1016/S1474-4422\(11\)70261-7](https://doi.org/10.1016/S1474-4422(11)70261-7)
- Holsbeeks, I., O. Lagatie, A. Van Nuland, S. Van de Velde, and J.M. Thevelein. 2004. The eukaryotic plasma membrane as a nutrient-sensing device. *Trends Biochem. Sci*. 29:556–564. <https://doi.org/10.1016/j.tics.2004.08.010>
- Jézégou, A., E. Llinares, C. Anne, S. Kieffer-Jaquinod, S. O'Regan, J. Aupetit, A. Chabli, C. Sagné, C. Debacker, B. Chadefaux-Vekemans, et al. 2012. Hep-tahelical protein PQLC2 is a lysosomal cationic amino acid exporter underlying the action of cysteamine in cystinosis therapy. *Proc. Natl. Acad. Sci. USA*. 109:E3434–E3443. <https://doi.org/10.1073/pnas.1211198109>
- Jung, J., H.M. Genau, and C. Behrends. 2015. Amino Acid-Dependent mTORC1 Regulation by the Lysosomal Membrane Protein SLC38A9. *Mol. Cell Biol*. 35:2479–2494. <https://doi.org/10.1128/MCB.00125-15>
- Jung, J., A. Nayak, V. Schaeffer, T. Starzetz, A.K. Kirsch, S. Müller, I. Dikic, M. Mittelbronn, and C. Behrends. 2017. Multiplex image-based autophagy RNAi screening identifies SMCR8 as ULK1 kinase activity and gene expression regulator. *eLife*. 6:e23063. <https://doi.org/10.7554/eLife.23063>
- Kalatzis, V., S. Cherqui, C. Antignac, and B. Gasnier. 2001. Cystinosis, the protein defective in cystinosis, is a H(+)-driven lysosomal cystine transporter. *EMBO J*. 20:5940–5949. <https://doi.org/10.1093/emboj/20.21.5940>
- Lee, Y., T. Nishizawa, K. Yamashita, R. Ishitani, and O. Nureki. 2015. Structural basis for the facilitative diffusion mechanism by SemiSWEET transporter. *Nat. Commun*. 6:6112. <https://doi.org/10.1038/ncomms7112>
- Levine, T.P., R.D. Daniels, A.T. Gatta, L.H. Wong, and M.J. Hayes. 2013. The product of C9orf72, a gene strongly implicated in neurodegeneration, is structurally related to DENN Rab-GEFs. *Bioinformatics*. 29:499–503. <https://doi.org/10.1093/bioinformatics/bts725>
- Liu, B., H. Du, R. Rutkowski, A. Gartner, and X. Wang. 2012. LAAT-1 is the lysosomal lysine/arginine transporter that maintains amino acid homeostasis. *Science*. 337:351–354. <https://doi.org/10.1126/science.1220281>
- Marat, A.L., H. Dokainish, and P.S. McPherson. 2011. DENN domain proteins: regulators of Rab GTPases. *J. Biol. Chem*. 286:13791–13800. <https://doi.org/10.1074/jbc.R110.217067>
- Markello, T.C., I.M. Bernardini, and W.A. Gahl. 1993. Improved renal function in children with cystinosis treated with cysteamine. *N. Engl. J. Med*. 328:1157–1162. <https://doi.org/10.1056/NEJM199304223281604>
- McAlpine, W., L. Sun, K.W. Wang, A. Liu, R. Jain, M. San Miguel, J. Wang, Z. Zhang, B. Hayse, S.G. McAlpine, et al. 2018. Excessive endosomal TLR signaling causes inflammatory disease in mice with defective SMCR8-WDR41-C9ORF72 complex function. *Proc. Natl. Acad. Sci. USA*. 115:E11523–E11531. <https://doi.org/10.1073/pnas.1814753115>

- McQuinn, C., A. Goodman, V. Chernyshev, L. Kametsky, B.A. Cimino, K.W. Karhohs, M. Doan, L. Ding, S.M. Rafelski, D. Thirstrup, et al. 2018. CellProfiler 3.0: Next-generation image processing for biology. *PLoS Biol.* 16:e2005970. <https://doi.org/10.1371/journal.pbio.2005970>
- Meng, J., and S.M. Ferguson. 2018. GATOR1-dependent recruitment of FLCN-FNIP to lysosomes coordinates Rag GTPase heterodimer nucleotide status in response to amino acids. *J. Cell Biol.* 217:2765–2776. <https://doi.org/10.1083/jcb.201712177>
- Menon, S., C.C. Dibble, G. Talbott, G. Hoxhaj, A.J. Valvezan, H. Takahashi, L.C. Cantley, and B.D. Manning. 2014. Spatial control of the TSC complex integrates insulin and nutrient regulation of mTORC1 at the lysosome. *Cell.* 156:771–785. <https://doi.org/10.1016/j.cell.2013.11.049>
- Nada, S., A. Hondo, A. Kasai, M. Koike, K. Saito, Y. Uchiyama, and M. Okada. 2009. The novel lipid raft adaptor p18 controls endosome dynamics by anchoring the MEK-ERK pathway to late endosomes. *EMBO J.* 28:477–489. <https://doi.org/10.1038/emboj.2008.308>
- O'Rourke, J.G., L. Bogdanik, A. Yáñez, D. Lall, A.J. Wolf, A.K. Muhammad, R. Ho, S. Carmona, J.P. Vit, J. Zarrow, et al. 2016. C9orf72 is required for proper macrophage and microglial function in mice. *Science.* 351:1324–1329. <https://doi.org/10.1126/science.aaf1064>
- Panchaud, N., M.P. Péli-Gulli, and C. De Virgilio. 2013. Amino acid deprivation inhibits TORC1 through a GTPase-activating protein complex for the Rag family GTPase Gtr1. *Sci. Signal.* 6:ra42. <https://doi.org/10.1126/scisignal.2004112>
- Petit, C.S., A. Rocznik-Ferguson, and S.M. Ferguson. 2013. Recruitment of folliculin to lysosomes supports the amino acid-dependent activation of Rag GTPases. *J. Cell Biol.* 202:1107–1122. <https://doi.org/10.1083/jcb.201307084>
- Pisoni, R.L., J.G. Thoene, and H.N. Christensen. 1985. Detection and characterization of carrier-mediated cationic amino acid transport in lysosomes of normal and cystinotic human fibroblasts. Role in therapeutic cystine removal? *J. Biol. Chem.* 260:4791–4798.
- Ran, F.A., P.D. Hsu, J. Wright, V. Agarwala, D.A. Scott, and F. Zhang. 2013. Genome engineering using the CRISPR-Cas9 system. *Nat. Protoc.* 8:2281–2308. <https://doi.org/10.1038/nprot.2013.143>
- Rebsamen, M., L. Pochini, T. Stasyk, M.E. de Araújo, M. Galluccio, R.K. Kandasamy, B. Snijder, A. Fauster, E.L. Rudashevskaya, M. Bruckner, et al. 2015. SLC38A9 is a component of the lysosomal amino acid sensing machinery that controls mTORC1. *Nature.* 519:477–481. <https://doi.org/10.1038/nature14107>
- Renton, A.E., E. Majounie, A. Waite, J. Simón-Sánchez, S. Rollinson, J.R. Gibbs, J.C. Schymick, H. Laaksovirta, J.C. van Swieten, L. Myllykangas, et al. ITALSGEN Consortium. 2011. A hexanucleotide repeat expansion in C9ORF72 is the cause of chromosome 9p21-linked ALS-FTD. *Neuron.* 72:257–268. <https://doi.org/10.1016/j.neuron.2011.09.010>
- Richardson, C.D., G.J. Ray, M.A. DeWitt, G.L. Currie, and J.E. Corn. 2016. Enhancing homology-directed genome editing by catalytically active and inactive CRISPR-Cas9 using asymmetric donor DNA. *Nat. Biotechnol.* 34:339–344. <https://doi.org/10.1038/nbt.3481>
- Sagné, C., C. Aguilhon, P. Ravassard, M. Darmon, M. Hamon, S. El Mestikawy, B. Gasnier, and B. Giros. 2001. Identification and characterization of a lysosomal transporter for small neutral amino acids. *Proc. Natl. Acad. Sci. USA.* 98:7206–7211. <https://doi.org/10.1073/pnas.121183498>
- Sancak, Y., T.R. Peterson, Y.D. Shaul, R.A. Lindquist, C.C. Thoreen, L. Bar-Peled, and D.M. Sabatini. 2008. The Rag GTPases bind raptor and mediate amino acid signaling to mTORC1. *Science.* 320:1496–1501. <https://doi.org/10.1126/science.1157535>
- Schindelin, J., I. Arganda-Carreras, E. Frise, V. Kaynig, M. Longair, T. Pietzsch, S. Preibisch, C. Rueden, S. Saalfeld, B. Schmid, et al. 2012. Fiji: an open-source platform for biological-image analysis. *Nat. Methods.* 9:676–682. <https://doi.org/10.1038/nmeth.2019>
- Sellier, C., M.L. Campanari, C. Julie Corbier, A. Gaucherot, I. Kolb-Cheyne, M. Oulad-Abdelghani, F. Ruffenach, A. Page, S. Ciura, E. Kabashi, and N. Charlet-Berguerand. 2016. Loss of C9ORF72 impairs autophagy and synergizes with polyQ Ataxin-2 to induce motor neuron dysfunction and cell death. *EMBO J.* 35:1276–1297. <https://doi.org/10.15252/embj.201593350>
- Shi, Y., S. Lin, K.A. Staats, Y. Li, W.H. Chang, S.T. Hung, E. Hendricks, G.R. Linares, Y. Wang, E.Y. Son, et al. 2018. Haploinsufficiency leads to neurodegeneration in C9ORF72 ALS/FTD human induced motor neurons. *Nat. Med.* 24:313–325. <https://doi.org/10.1038/nm.4490>
- Shimobayashi, M., and M.N. Hall. 2014. Making new contacts: the mTOR network in metabolism and signalling crosstalk. *Nat. Rev. Mol. Cell Biol.* 15:155–162. <https://doi.org/10.1038/nrm3757>
- Sivadasan, R., D. Hornburg, C. Drepper, N. Frank, S. Jablonka, A. Hansel, X. Lojewski, J. Sternecker, A. Herrmann, P.J. Shaw, et al. 2016. C9ORF72 interaction with cofilin modulates actin dynamics in motor neurons. *Nat. Neurosci.* 19:1610–1618. <https://doi.org/10.1038/nn.4407>
- Sullivan, P.M., X. Zhou, A.M. Robins, D.H. Paushter, D. Kim, M.B. Smolka, and F. Hu. 2016. The ALS/FTLD associated protein C9orf72 associates with SMC8 and WDR41 to regulate the autophagy-lysosome pathway. *Acta Neuropathol. Commun.* 4:51. <https://doi.org/10.1186/s40478-016-0324-5>
- Tharkeshwar, A.K., J. Trekker, W. Vermeire, J. Pauwels, R. Sannerud, D.A. Priestman, D. Te Vruchte, K. Vints, P. Baatsen, J.P. Decuyper, et al. 2017. A novel approach to analyze lysosomal dysfunctions through subcellular proteomics and lipidomics: the case of NPC1 deficiency. *Sci. Rep.* 7:41408. <https://doi.org/10.1038/srep41408>
- Thevelein, J.M., and K. Voordeckers. 2009. Functioning and evolutionary significance of nutrient transceptors. *Mol. Biol. Evol.* 26:2407–2414. <https://doi.org/10.1093/molbev/msp168>
- Thoene, J.G., R.G. Oshima, J.C. Crawhall, D.L. Olson, and J.A. Schneider. 1976. Cystinosis. Intracellular cystine depletion by amino thiols in vitro and in vivo. *J. Clin. Invest.* 58:180–189. <https://doi.org/10.1172/JCI108448>
- Town, M., G. Jean, S. Cherqui, M. Attard, L. Forestier, S.A. Whitmore, D.F. Callen, O. Gribouval, M. Broyer, G.P. Bates, et al. 1998. A novel gene encoding an integral membrane protein is mutated in nephropathic cystinosis. *Nat. Genet.* 18:319–324. <https://doi.org/10.1038/ng0498-319>
- Tsun, Z.Y., L. Bar-Peled, L. Chantranupong, R. Zoncu, T. Wang, C. Kim, E. Spooner, and D.M. Sabatini. 2013. The folliculin tumor suppressor is a GAP for the RagC/D GTPases that signal amino acid levels to mTORC1. *Mol. Cell.* 52:495–505. <https://doi.org/10.1016/j.molcel.2013.09.016>
- Ugolino, J., Y.J. Ji, K. Conchina, J. Chu, R.S. Nirujogi, A. Pandey, N.R. Brady, A. Hamacher-Brady, and J. Wang. 2016. Loss of C9orf72 Enhances Autophagic Activity via Deregulated mTOR and TFEF Signaling. *PLoS Genet.* 12:e1006443. <https://doi.org/10.1371/journal.pgen.1006443>
- Viodé, A., C. Fournier, A. Camuzat, F. Fenaillé, M. Latouche, F. Elahi, I. Le Ber, C. Junot, F. Lamari, V. Anquetil, and F. Becher. NeuroCEB Brain Bank. 2018. New Antibody-Free Mass Spectrometry-Based Quantification Reveals That C9ORF72 Long Protein Isoform Is Reduced in the Frontal Cortex of Hexanucleotide-Repeat Expansion Carriers. *Front. Neurosci.* 12:589. <https://doi.org/10.3389/fnins.2018.00589>
- Waite, A.J., D. Baumer, S. East, J. Neal, H.R. Morris, O. Anson, and D.J. Blake. 2014. Reduced C9orf72 protein levels in frontal cortex of amyotrophic lateral sclerosis and frontotemporal degeneration brain with the C9ORF72 hexanucleotide repeat expansion. *Neurobiol. Aging.* 35:1779.e5–1779.e13. <https://doi.org/10.1016/j.neurobiolaging.2014.01.016>
- Wang, T., J.J. Wei, D.M. Sabatini, and E.S. Lander. 2014. Genetic screens in human cells using the CRISPR-Cas9 system. *Science.* 343:80–84. <https://doi.org/10.1126/science.1246981>
- Wang, S., Z.Y. Tsun, R.L. Wolfson, K. Shen, G.A. Wyant, M.E. Plovnick, E.D. Yuan, T.D. Jones, L. Chantranupong, W. Comb, et al. 2015. Metabolism. Lysosomal amino acid transporter SLC38A9 signals arginine sufficiency to mTORC1. *Science.* 347:188–194. <https://doi.org/10.1126/science.1257132>
- Webster, C.P., E.F. Smith, C.S. Bauer, A. Moller, G.M. Hautbergue, L. Ferraiuolo, M.A. Myszczyńska, A. Higginbottom, M.J. Walsh, A.J. Whitworth, et al. 2016. The C9orf72 protein interacts with Rab1a and the ULK1 complex to regulate initiation of autophagy. *EMBO J.* 35:1656–1676. <https://doi.org/10.15252/embj.201694401>
- Wolfson, R.L., and D.M. Sabatini. 2017. The Dawn of the Age of Amino Acid Sensors for the mTORC1 Pathway. *Cell Metab.* 26:301–309. <https://doi.org/10.1016/j.cmet.2017.07.001>
- Wu, X., M.J. Bradley, Y. Cai, D. Kümmel, E.M. De La Cruz, F.A. Barr, and K.M. Reinisch. 2011. Insights regarding guanine nucleotide exchange from the structure of a DENN-domain protein complexed with its Rab GTPase substrate. *Proc. Natl. Acad. Sci. USA.* 108:18672–18677. <https://doi.org/10.1073/pnas.1110415108>
- Xi, Z., L. Zinman, D. Moreno, J. Schymick, Y. Liang, C. Sato, Y. Zheng, M. Ghani, S. Dib, J. Keith, et al. 2013. Hypermethylation of the CpG island near the G4C2 repeat in ALS with a C9orf72 expansion. *Am. J. Hum. Genet.* 92:981–989. <https://doi.org/10.1016/j.ajhg.2013.04.017>
- Xiao, S., L. MacNair, J. McLean, P. McGoldrick, P. McKeever, S. Soleimani, J. Keith, L. Zinman, E. Rogaeva, and J. Robertson. 2016. C9orf72 isoforms in Amyotrophic Lateral Sclerosis and Frontotemporal Lobar Degeneration. *Brain Res.* 1647:43–49. <https://doi.org/10.1016/j.brainres.2016.04.062>
- Xuan, Y.H., Y.B. Hu, L.Q. Chen, D. Sosso, D.C. Ducat, B.H. Hou, and W.B. Frommer. 2013. Functional role of oligomerization for bacterial and plant SWEET sugar transporter family. *Proc. Natl. Acad. Sci. USA.* 110:E3685–E3694. <https://doi.org/10.1073/pnas.1311244110>

- Yang, M., C. Liang, K. Swaminathan, S. Herrlinger, F. Lai, R. Shiekhattar, and J.F. Chen. 2016. A C9ORF72/SMCR8-containing complex regulates ULK1 and plays a dual role in autophagy. *Sci. Adv.* 2:e1601167. <https://doi.org/10.1126/sciadv.1601167>
- Zhai, Y., W.H. Heijne, D.W. Smith, and M.H. Saier Jr. 2001. Homologues of archaeal rhodopsins in plants, animals and fungi: structural and functional predications for a putative fungal chaperone protein. *Biochim. Biophys. Acta.* 1511:206-223. [https://doi.org/10.1016/S0005-2736\(00\)00389-8](https://doi.org/10.1016/S0005-2736(00)00389-8)
- Zhang, D., L.M. Iyer, F. He, and L. Aravind. 2012. Discovery of Novel DENN Proteins: Implications for the Evolution of Eukaryotic Intracellular Membrane Structures and Human Disease. *Front. Genet.* 3:283. <https://doi.org/10.3389/fgene.2012.00283>
- Zhang, Y., A. Burberry, J.Y. Wang, J. Sandoe, S. Ghosh, N.D. Udeshi, T. Svinkina, D.A. Mordes, J. Mok, M. Charlton, et al. 2018. The C9orf72-interacting protein Smcr8 is a negative regulator of autoimmunity and lysosomal exocytosis. *Genes Dev.* 32:929-943. <https://doi.org/10.1101/gad.313932.118>

Supplemental material

Amick et al., <https://doi.org/10.1083/jcb.201906076>

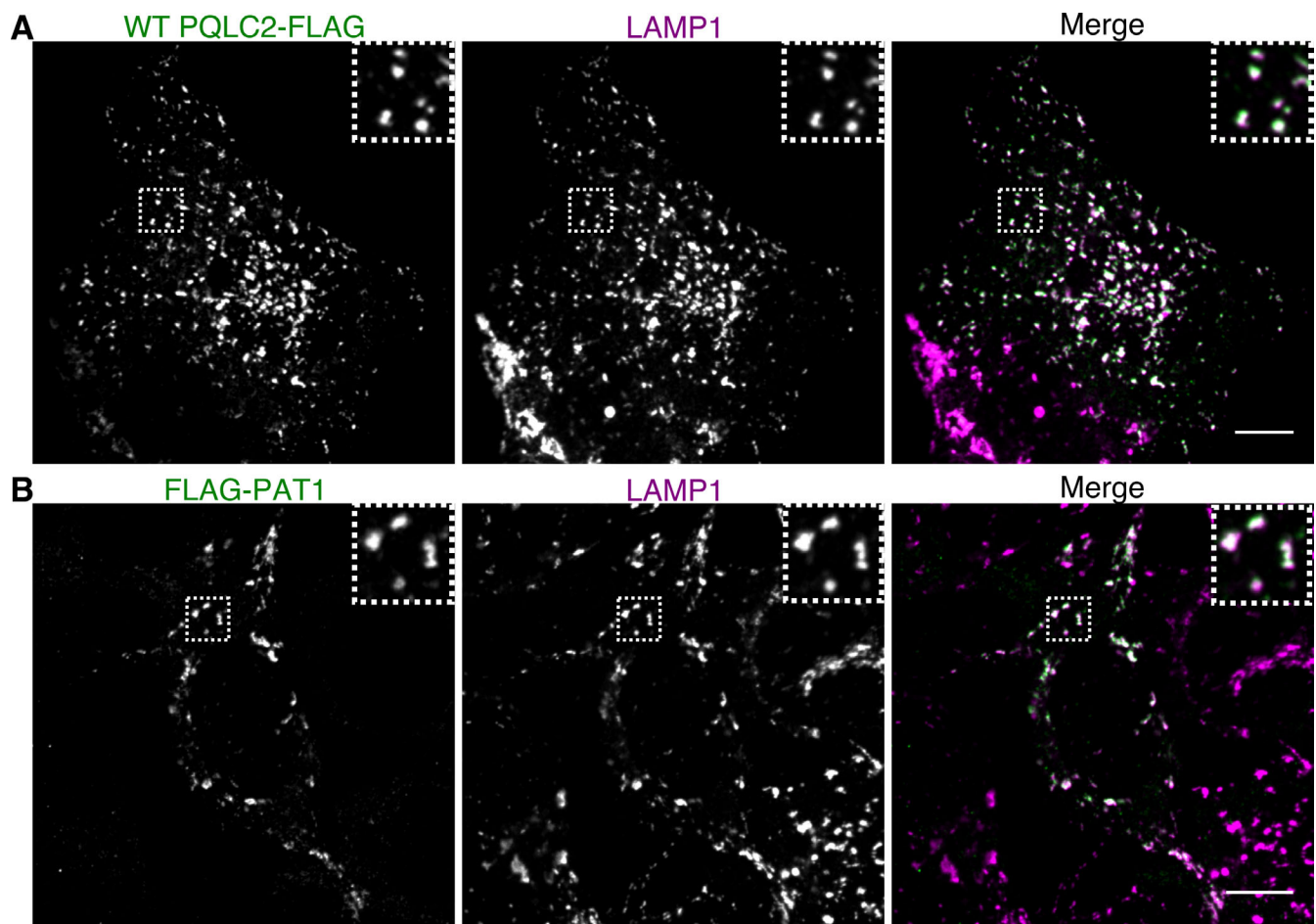


Figure S1. **PQLC2-FLAG and FLAG-PAT1 localize to lysosomes.** (A and B) Immunofluorescence images of FLAG and LAMP1 in HEK293FT cells transiently transfected with FLAG-tagged PQLC2 (A) or PAT1 (B). Scale bars: 10  $\mu$ m. Inset is 7.6  $\mu$ m wide in A and 6.7  $\mu$ m wide in B.

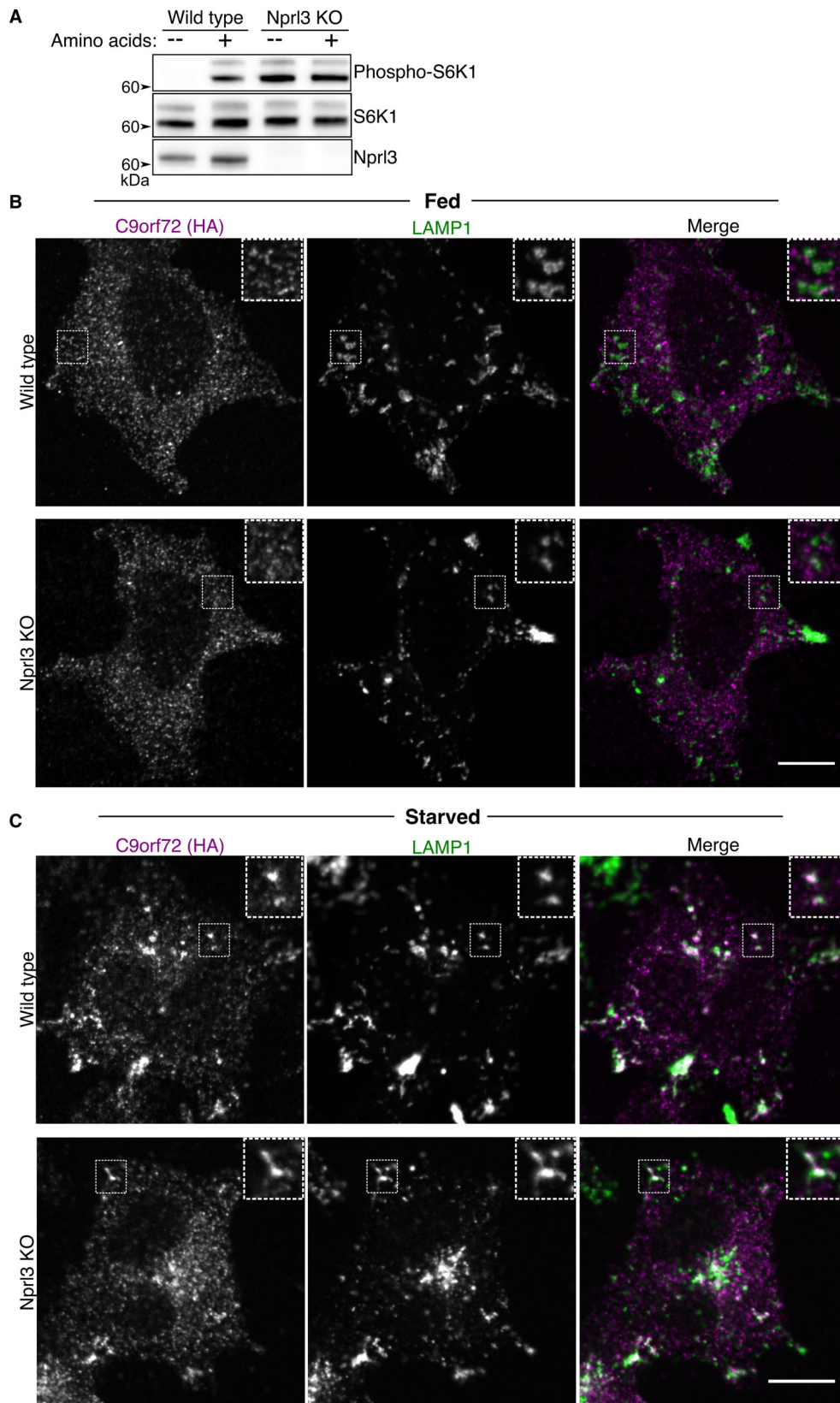


Figure S2. **C9orf72 recruitment to lysosomes is independent of GATOR1-associated nutrient sensing.** (A) Immunoblot analysis of Nprl3, S6K, and phospho-S6K (T389) levels during starvation (2 h) and amino acid refeeding (15 min) in WT and Nprl3 KO cells. (B) Immunofluorescence images of C9orf72 localization under normal growth conditions for WT and Nprl3 KO cells. Insets are 5.5  $\mu$ m wide. (C) Immunofluorescence images of C9orf72 localization under starved conditions (2 h) for WT and Nprl3 KO cells. Localization of C9orf72 to late endosomes and lysosomes is demonstrated by colocalization with LAMP1 puncta. Scale bars: 10  $\mu$ m. Insets are 4.8  $\mu$ m wide.

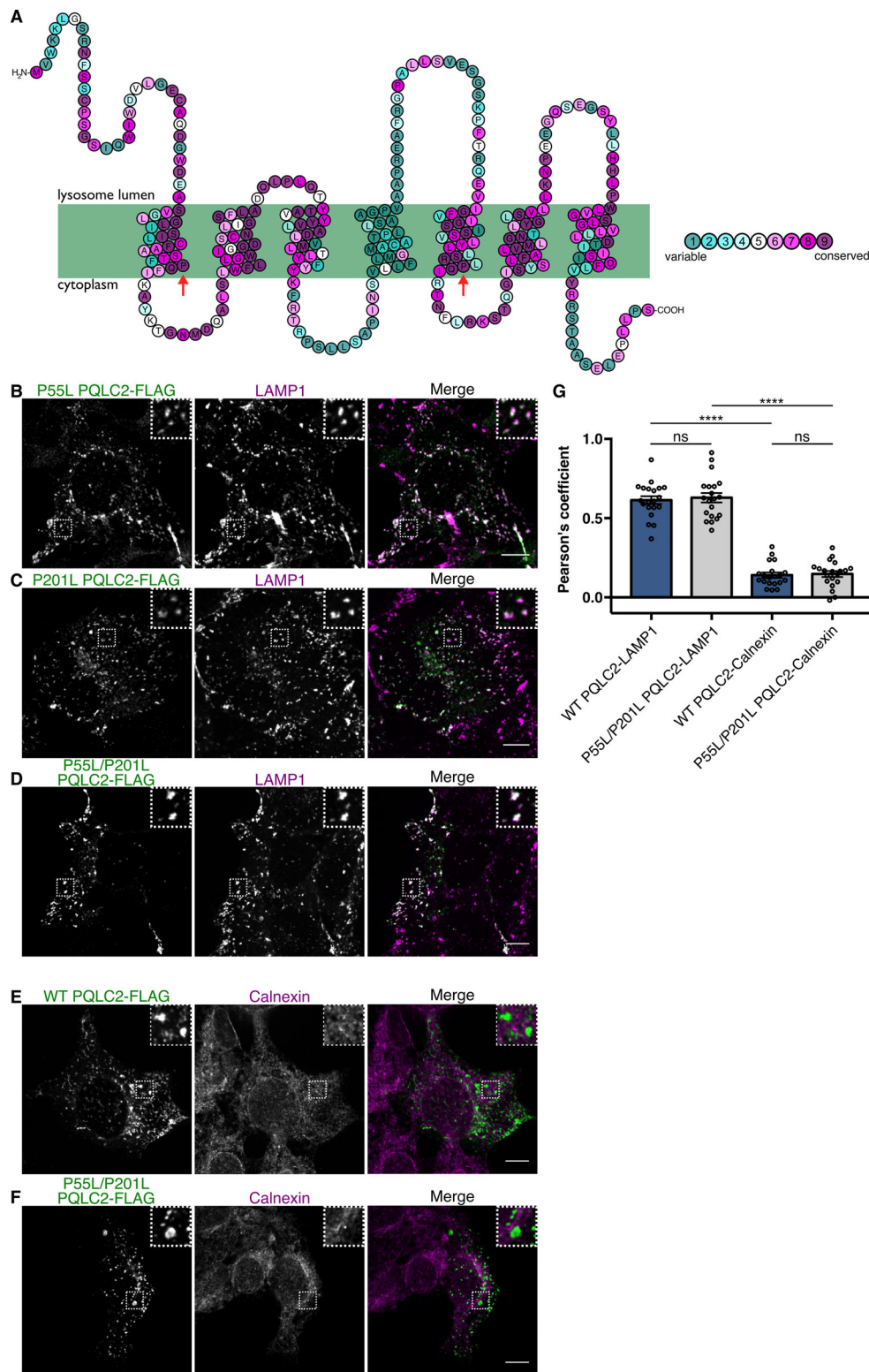


Figure S3. **PQLC2-FLAG PQ loop mutants localize to lysosomes.** (A) Visualization of PQLC2 topology generated by Protter overlaid with the conservation of amino acids at each position from ConSurf (Ashkenazy et al., 2016). The positions of the prolines in the PQ loops are indicated by arrows. (B–D) Immunofluorescence images of FLAG and LAMP1 labeling in HEK293FT cells transiently transfected with FLAG-tagged PQLC2 mutants: P55L (B), P201L (C), and P55L/P201L (D). Scale bars: 10  $\mu$ m. Insets are 6.4  $\mu$ m wide in B, 6.8  $\mu$ m wide in C, and 7.7  $\mu$ m wide in D. (E and F) Immunofluorescence images of FLAG and calnexin localization in cells transfected with FLAG-tagged WT PQLC2 (E) and P55L/P201L mutant PQLC2 (F). Scale bars: 10  $\mu$ m. Insets are 7.7  $\mu$ m wide in E and F. (G) Quantification of WT and mutant PQLC2 colocalization with LAMP1 and calnexin (images of WT PQLC2 and LAMP1 colocalization are shown in Fig. S1). Pearson's correlation coefficient was measured with results from individual images plotted as open circles; mean  $\pm$  SEM, ANOVA with Tukey's multiple comparisons test. \*\*\*\*,  $P \leq 0.0001$ ,  $n = 3$  experiments with a total of 20 images analyzed.

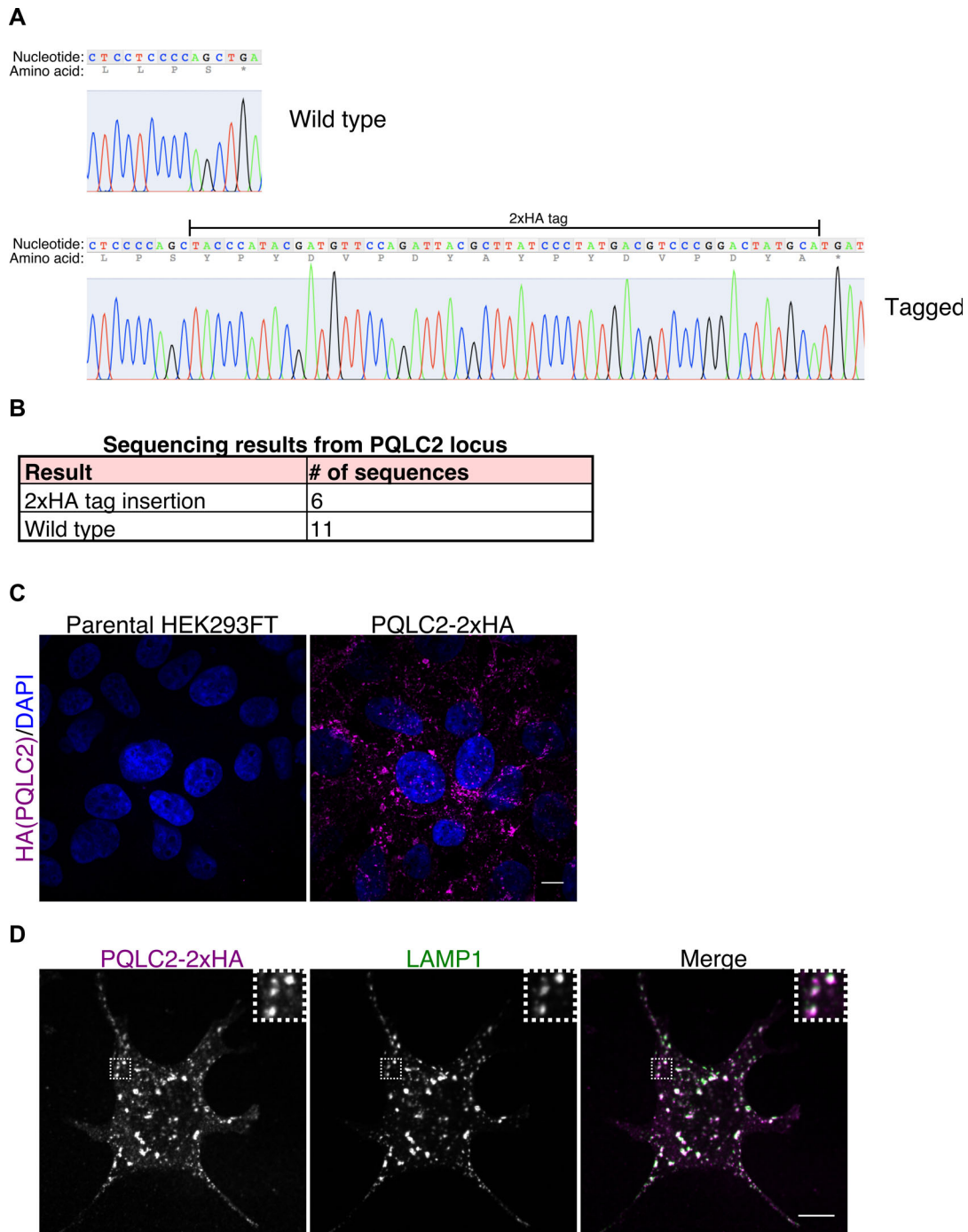


Figure S4. **Epitope tagging of the endogenous PQLC2 protein.** (A) Sequencing traces from an HEK293FT cell line that has a 2xHA epitope tag inserted into the endogenous PQLC2 gene. Example traces from unaffected and edited alleles are shown. This insertion results in a 2xHA tag at the C-terminus of PQLC2. (B) Summary of sequencing results from this cell line. Results are consistent with one of three copies of PQLC2 being 2xHA-tagged at the C-terminus, while the remaining two copies of the gene are unaffected. (C) The specificity of the anti-HA immunofluorescence signal in PQLC2-2xHA cells is supported by the absence of this signal in parental, non-gene-edited cells. (D) Immunofluorescence images showing the localization of PQLC2-2xHA to lysosomes (endogenous PQLC2-2xHA and LAMP1). Scale bars: 10  $\mu$ m. Insets are 5.9  $\mu$ m wide.

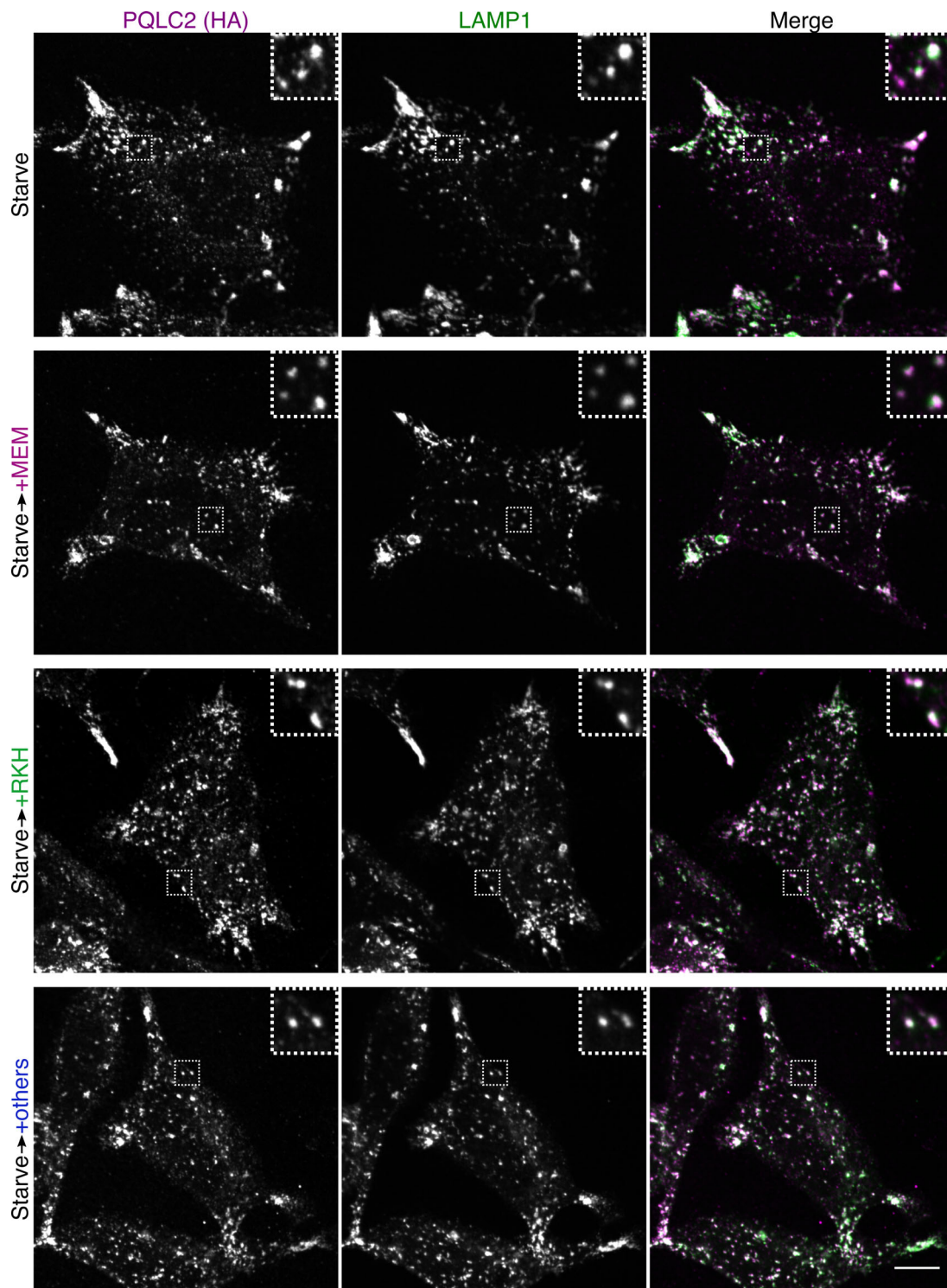


Figure S5. **PQLC2 localization to lysosomes is not regulated by changes in amino acid availability.** Immunofluorescence images of PQLC2-2xHA and LAMP1 in cells expressing PQLC2-2xHA from the endogenous locus. Cells were starved and then incubated in media containing the indicated amino acids (as in Figs. 4 F and 5). Scale bar: 10  $\mu$ m. Insets are 5.7  $\mu$ m wide.

Four tables and one dataset are provided online. Table S1 lists the DNA sequences used for generating the plasmids used in this study. Table S2 provides a list of the antibodies used in this study. Table S3 contains the primers used for PCR amplification of genomic DNA. Table S4 contains the sequences used for the PQLC2 CRISPR knockin. Dataset 1 contains the gBlock sequence used to generate the PQLC2-FLAG plasmids.